

NACA TN 4062 96301

0066933

TECH LIBRARY KAFB, NM

NATIONAL ADVISORY COMMITTEE FOR AERONAUTICS

TECHNICAL NOTE 4062

EFFECT OF SWEEP ON PERFORMANCE OF COMPRESSOR BLADE
SECTIONS AS INDICATED BY SWEPT-BLADE ROTOR,
UNSWEPT-BLADE ROTOR, AND CASCADE TESTS

By William R. Godwin

Langley Aeronautical Laboratory
Langley Field, Va.



Washington
July 1957

TECHNICAL LIBRARY
AFL 2811



TECHNICAL NOTE 4062

EFFECT OF SWEEP ON PERFORMANCE OF COMPRESSOR BLADE

SECTIONS AS INDICATED BY SWEEP-BLADE ROTOR,

UNSWEPT-BLADE ROTOR, AND CASCADE TESTS

By William R. Godwin

SUMMARY

An investigation has been made to determine the induced effect of sweep on an axial-flow compressor blade. Velocities of entering and exiting flow and blade-section pressure distributions were measured at three radial stations on a 30° swept-blade rotor of 0.69 hub-tip ratio having the same blade geometric characteristics as an NACA 65-series unswept-blade rotor for which similar quantities were measured and the results presented in NACA Technical Note 3806. In these tests, the blade tip speed was 183 feet per second and the inlet Mach number relative to the rotor ranged from 0.25 to 0.45. The blade-section pressure distributions were obtained by the use of a mercury-seal pressure-transfer device. The data obtained were also compared with similar data for the same blade sections obtained from a two-dimensional porous-wall cascade tunnel.

The comparisons of blade-section pressure distributions indicated that, in order to obtain the same effective angles of attack on the swept-blade rotor as on the unswept-blade rotor, the swept blade would require an additional twist of 3.8° for the entire radial span. Two-dimensional cascade data adequately predicted the turning angle through the swept-blade rotor if the change in axial velocity provided by the trailing portion of the blade was taken into account.

INTRODUCTION

In axial-flow compressors, the demand for higher weight flows and fewer stages has led to higher inlet Mach numbers relative to the compressor blade. When the Mach number is increased much above the critical Mach number, the blade losses usually go up. Still further increases in Mach number usually lead to choking of the flow, particularly for blade sections of high solidity, high thickness, and low inlet air angle. The application of sweepback has been suggested as a possible means of increasing the inlet Mach number range. Sweepback is not expected to

increase appreciably the critical Mach number for compressor blades as it does for aircraft wings because the spanwise flow will be restrained by the inner and outer casings. Sweepback, however, can increase the minimum flow area in the blade passage and in that way may extend the usable Mach number range.

Sweepback presents aerodynamic problems in blade design as well as the mechanical problem of high stress. Sweeping the blade causes a spanwise variation in induced velocity at the leading edge and also causes a change of several percent in axial velocity ahead of and behind the blade.

In order to determine the detailed effects of sweep on a rotating blade, blade-section pressure distributions would be necessary. Pressure distributions on an unswept blade have been reported in reference 1. In the present investigation, pressure distributions were measured for a swept blade with other geometric characteristics similar to the blade tested in reference 1. No attempt was made to correct the spanwise blade loading for sweep. The differences in the pressure distributions of the swept and unswept blades should indicate the induced effects produced by sweeping the blade. The tests covered a Mach number range from 0.25 to 0.45.

SYMBOLS

| | |
|----------------|--|
| c | chord, ft |
| c_n | section normal-force coefficient (normal to chord) |
| $c_{n,M}$ | section normal-force coefficient, from measured change in momentum and static pressure |
| $c_{n,P}$ | section normal-force coefficient, from area of pressure distribution |
| $c_{n,\theta}$ | section normal-force coefficient, from corrected θ, α curve |
| M | Mach number |
| p | static pressure, lb/sq ft |
| P | total pressure, lb/sq ft |
| q | dynamic pressure, $\frac{1}{2}\rho V^2$, lb/sq ft |
| t | thickness, ft |

| | |
|-----------|---|
| U | rotational velocity of rotor blade at any radius, ft/sec |
| V | velocity, ft/sec |
| α | angle of attack (angle between entering air and chord line), deg |
| α' | angle of attack corrected to average axial velocity |
| β | inlet air angle (angle between entering air and axial direction), deg |
| θ | turning angle (angle through which air is turned by blade element), deg |
| θ' | turning angle corrected to average axial velocity |
| ρ | density, slugs/cu ft |

Subscripts:

| | |
|---|---------------------------------------|
| 0 | station ahead of guide vanes |
| 1 | station between guide vanes and rotor |
| 2 | station behind rotor |
| a | axial |
| l | local chordwise point |
| n | normal to blade leading edge |
| p | similar pressure distribution |
| q | similar flow quantity |
| r | relative to rotor |
| s | swept blade |
| u | unswept blade |

APPARATUS AND TESTS

The axial-flow test compressor with a tip diameter of 42 inches used for the present investigation is shown in figure 1. The major

alteration to the general configuration since the work of reference 1 was the replacement of the conical diffuser by two 90° diffusing cascade bends. These bends slightly reduced the weight flow for the open-throttle conditions.

Blading

A sketch of the rotor blades is shown in figure 2. The blades, 24 in all, were swept versions of the blades discussed in reference 1. The angle of sweep was 30° and the twist, blade sections, solidity, and blade-setting angle were the same as those for the unswept blade. Three blades, each containing 24 static-pressure orifices, were used for measuring pressure distributions. The orifices were located at the outboard, mean, and inboard sections as in reference 1, the outboard and inboard sections being located 1 inch from the ends of the blade. The span of the blade is reduced at the trailing edge because of the combined effects of the blade sweep and blade-setting angle. The dashed lines in figure 2 show estimated streamlines for the swept rotor. The blade had a radial span of 6.5 inches and a constant chord of 5.5 inches normal to a radial line. The blade-tip clearance was approximately 0.030 inch. The blade sections tested are described in the following table:

| | Outboard | Mean | Inboard |
|------------------------------------|----------|-------|---------|
| Camber | 1.096 | 1.200 | 1.304 |
| Solidity | 1.050 | 1.183 | 1.355 |
| Blade-setting angle, deg | 48.1 | 46.1 | 44.7 |
| Thickness ratio, t/c | 0.10 | 0.10 | 0.10 |

The blade-setting angle is measured between the chord line and the axis of rotation. Vector diagrams for the original design conditions are shown in figure 3.

The row of guide vanes was the same as that used with the unswept blade of reference 1. They produced a free-vortex velocity profile against the direction of rotation as the flow entered the rotor.

Instrumentation

The 24-cell, mercury-seal, pressure-transfer device was the same as that used in reference 1.

The airspeed and flow direction between the guide vanes and rotor and behind the rotor were measured with automatic yaw instruments containing a pressure probe having null-type yaw, static-pressure, and

total-pressure elements. The probes were of the form referred to as prism probes in reference 2 with the yaw tubes cut at an angle of 45° for greater sensitivity.

Method of Testing

Blade pressure distribution, total pressure, static pressure, and flow direction ahead of and behind the rotor were measured at six angles of attack at the outboard section and at eight angles of attack at the mean and inboard sections for a tip speed of 183 feet per second. The angle of attack at the mean diameter was varied from 9.7° up to the stall point by throttling the discharge. The throttle was adjusted until the dynamic pressure at the mean radius ahead of the guide vanes, q_0 , closely approximated q_0 for the unswept-blade tests. All pressure measurements including blade pressure distributions at a given blade section were recorded simultaneously by photographing a multitube manometer board.

RESULTS AND DISCUSSION

Blade-Section Pressure Distributions

For a comparison of the unswept- and swept-blade sections, pressure distributions for the same q_0 and rotational speed were superimposed for each of the three sections. The comparisons were made at three conditions covering the operating range: open throttle, design, and near surge. The slight differences in angle of attack at corresponding values of q_0 for the comparisons may be attributed to a slight radial variation in axial velocity for the swept case and the effect of small fluctuations in the flow on the measured air angle at station 1.

In figure 4, the comparisons are for the outboard section. The first comparison is for the open-throttle or low-angle-of-attack condition. The upper surface curve is more peaked toward the leading edge and the lower surface curve is less peaked for the swept case than for the unswept case. This condition indicates that the swept-blade section is operating at an effectively higher angle of attack than the unswept section. In the design and near-surge plots (figs. 4(b) and (c)), it can be seen from the upper and lower surface curves near the leading edge that the swept blade continued to operate at an effectively higher angle of attack than the unswept blade over the measured operating range.

At the mean section (fig. 5), the comparison indicates that the effective angles of attack are very similar for the swept and unswept sections over the measured operating range, the peaks on both surfaces being in close agreement.

At the inboard section (fig. 6), the pressure distributions indicate that the swept blade was operating at a lower effective angle of attack than the unswept blade over the measured operating range.

Matching Pressure Distributions

By comparing pressure distributions at slightly different angles of attack, it was possible to obtain pressure distributions for the unswept blade that were similar to those for the swept blade. In most cases, the measured pressure distributions for the unswept blade bracketed the pressure distribution for the swept blade; a linear interpolation was used on the ordinate and the parameters $M_{1,r}$, α , θ , and q_0 at the desired pressure distribution.

In figure 7, matching pressure distributions are shown for the outboard sections of the swept and unswept blades covering the same operating conditions as the swept blade in figure 4. Figure 8 provides similarly matched pressure distributions for the inboard sections. At the mean section, further comparison of the pressure distributions was deemed unnecessary.

Thus, for each pressure distribution on the swept blade, two related pressure distributions can be obtained on the unswept blade - one having a similar distribution and the other having a similar throttle setting as indicated by q_0 . The change in angle of attack for the unswept blade in going from the same throttle setting to the same pressure distribution as the swept blade provides an approximate value for the change in effective angle of attack due to sweeping the blade. The throttle setting (i.e., q_0) was used as a basis of comparison rather than angle of attack as computed from instrument measurements at station 1 because q_0 could be measured accurately, whereas measurements at station 1 were less accurate because of the effects of the radial flows and the guide-vane wakes.

The matching process was used for all the points tested at the three sections of the blade. From plots of q_0 against angle of attack for the unswept blade, the change in induced angle was approximated by the difference in angle of attack of the unswept blade under the two q_0 conditions of the matching pressure distributions. The results of this process are shown in figure 9 and indicate that, in order to obtain the design angle of attack at all radii, the blade twist should be increased by 2.6° between the inboard and outboard sections or 0.58° per inch of radial span. The increase in twist amounts to approximately 3.8° for the overall radial span. Although twisting the blade as suggested by the data of figure 9 would reduce the lift at the tip and increase it at the hub so that the required twist at the outboard section and inboard section would be reduced, the difference in twist is negligible for this rotor. Also presented in figure 9 are predicted values of twist for the design condition for an isolated airfoil estimated from the charts of reference 3.

On the swept-blade rotor at the leading edge of each blade section, the cross-sectional-flow area of the airstream is somewhat reduced by the cross-sectional area of the blade inboard of that section. This reduction in area would result in a higher axial velocity at the leading edge of the swept blade than for the unswept blade. At the instrument stations upstream of the blade, the passage areas for the two blades, and hence the axial velocities, were the same for the same q_0 . This condition indicates that there was a change in axial velocity in the swept-blade rotor that was not present in the unswept-blade rotor between the upstream measuring station and the blade leading edge.

A calculation of the increase in axial velocity at the blade leading edge was made for the three blade sections by using the reduction in area due to the thickness of the swept blade inboard of each section. The velocities measured at the instrument location were converted to velocities at the blade leading edge by means of this increase in axial velocity. From the change in axial velocity, the change in angle of attack due to the thickness of the blade was obtained. These values were combined with the values of change in angle of attack due to sweep (fig. 9) to obtain the induced effect of sweep due to lift alone; the results are shown in figure 10. As can be seen from a comparison of figures 9 and 10, the thickness of the blade reduced the induced effect of sweep; in this case the reduction in twist was from 5.1° to 2.6° between the outboard and inboard sections, or about 50 percent.

Comparison of Turning Angles in Compressor and Cascade

Plots of turning angle against angle of attack of the blade sections for the swept-blade rotor and two-dimensional cascade are presented in figure 11. The compressor values were obtained from instrument measurements as they were for the unswept blade of reference 1, figure 11. The cascade values were taken from reference 4 and were determined by the carpet-plotting technique. For the outboard section, the camber for the swept blade was slightly greater than it had been for the unswept blade. This difference was caused by the shortening of the circumferential chord length at the outboard section by about 4 percent due to sweep and an increase in the maximum height of the mean line of about 3 percent due to radial twist of the blade. (See fig. 2.)

The outboard section (fig. 11(a)) of the swept-blade rotor provided 1.5° greater turning than was predicted by the cascade data for the same angle of attack. For the unswept-blade rotor, the turning was about 1° higher than that predicted by cascade. For the mean section, the swept-blade rotor provided 0.3° less turning at the design condition than was indicated by the cascade (fig. 11(b)). At the inboard section (fig. 11(c)), the swept-blade rotor provided approximately 2.5° less turning at design than indicated by the cascade, whereas for the unswept blade the rotor turning matched the cascade turning at design.

On the swept-blade rotor at the trailing edge of each blade section, the cross-sectional area of the airstream is reduced by the cross-sectional area of the blade as previously mentioned in regard to the leading edge. A calculation of the increase in axial velocity at the blade trailing edge was made for the three blade sections by using the reduction in area due to the presence of the trailing portion of the swept blade outboard of each section, and the velocities measured at the instrument downstream were converted to velocities at the blade trailing edge by increasing the component of the axial velocity. The results indicated an increase in turning angle of 0.4° , 1.2° , and 2.5° for the outboard, mean, and inboard sections, respectively, at the trailing edge as compared with the downstream station. Admittedly, the calculation for the change in axial velocity ignored many factors; the results, however, indicate a method of applying cascade data to the selection of blade sections in the design of swept-blade rotors.

Corrected Turning Angles

The angles of attack and turning angles were also corrected by using the mean-axial-velocity correction as in reference 1. The corrected curves are shown in figure 12. The correction considerably improved the agreement in turning angle between the swept-blade rotor and cascade at the outboard section which had a 5-percent lower axial velocity ahead of the rotor and a 5-percent higher exit axial velocity than the average axial velocity of the compressor. If the swept-blade turning angles were increased by the estimated change in turning between the trailing edge and instrument station, it appears that the agreement in turning angle between the swept-blade rotor and cascade would be the same as the agreement for the unswept-blade rotor and cascade for a region extending about 3° on either side of the design value.

The swept-blade turning-angle curves were also calculated for sections normal to the leading edge by using the data of figure 11 and the equations

$$\alpha_n = \tan^{-1} \frac{\tan \alpha}{\cos \Lambda}$$

and

$$\theta_n = \tan^{-1} \frac{\tan(\theta - \alpha)}{\cos \Lambda} + \alpha_n$$

where Λ is the sweepback angle. Also, cascade values were obtained from reference 4 for the "normal" blade parameters calculated from the following equations:

$$\beta_{1,n} = \tan^{-1} \left[\tan(\beta_1 - \alpha) \cos \Lambda \right] + \alpha_n$$

$$(C_{l,0})_n = \frac{C_{l,0}}{\cos \Lambda}$$

$$\sigma_n = \frac{\sigma}{\sqrt{\frac{\cos^2(\beta_1 - \alpha)}{\cos^2 \Lambda} + \sin^2(\beta_1 - \alpha)}}$$

where $C_{l,0}$ is the blade camber in terms of the isolated-airfoil lift coefficient and σ is the ratio of blade chord to blade gap. (These equations were derived by Melvyn Savage while at the Langley Aeronautical Laboratory and are based on cross sections taken through a cascade.) The resulting values of turning angle are shown in figure 13 and the agreement is about the same as that of figure 11, except that the cascade is operating nearer stall for the data of figure 13 than for the data of figure 11 at all three sections.

These comparisons of turning angle indicate that the differences in cascade and rotor inlet and exit air-flow angles were approximately of the same magnitude for both the swept-blade and unswept-blade rotors, provided that the inlet and exit air angles relative to the rotor are corrected by using the mean axial velocity correction and that in the swept case the change in axial velocity between the trailing edge and instrument measuring station is taken into account. The comparisons of cascade data and the data of swept-blade sections normal to the leading edge showed as good agreement in turning angle as similar comparisons based on blade sections parallel to the air flow at the cascade design angle of attack; however, the cascade values for the normal section did not adequately predict the higher than design angle-of-attack operating range.

Normal-Force Coefficients

As in reference 1, the normal-force coefficients were computed by three methods: (1) integration of measured pressure distributions, (2) from the measured changes in momentum and static pressure neglecting the drag force, and (3) from the inlet angle and turning angle by assuming

constant axial velocity with no loss in total pressure. The normal-force coefficients computed by these methods are designated $c_{n,P}$, $c_{n,M}$, and $c_{n,\theta}$ and are shown plotted in figure 14. At the outboard section, the pressure distributions $c_{n,P}$ indicate a higher loading than the measured momentum plus pressure rise $c_{n,M}$ indicates. The values of $c_{n,P}$ appear to be higher than the values of $c_{n,M}$ because of the increase in induced angle of attack with sweep. If the turning angles for the values of $c_{n,P}$ were computed on the basis of the effective angle of attack rather than the measured angle of attack, the values of $c_{n,P}$ would be in close agreement with the values of $c_{n,M}$. The values of $c_{n,\theta}$ are greater than the values of $c_{n,M}$ since $c_{n,\theta}$ was computed by using the ideal pressure rise.

At the mean section, the values of $c_{n,P}$ are also higher than the values of $c_{n,M}$. At this section, the change in induced angle of attack due to sweep is 0.5° or less, and shifting the values of $c_{n,P}$ accordingly would not appreciably change the agreement between $c_{n,P}$ and $c_{n,M}$.

For the inboard section, the agreement between $c_{n,P}$ and $c_{n,M}$ is close. Plotting the values of $c_{n,P}$ against θ corrected for the induced effect will not alter the agreement at this section, since the values of $c_{n,M}$ are nearly constant for high turning angles where the induced effect is greatest.

CONCLUSIONS

An investigation has been made to determine the induced effect of sweep on an axial-flow compressor which had its blades swept back 30° . All other geometric characteristics of this rotor were the same as those of the unswept-blade rotor described in NACA Technical Note 3806. The data of the tests cover a range in inlet Mach number relative to the rotor from 0.25 to 0.45. From comparisons of the pressure distributions on the swept and unswept blades and from comparisons of cascade and swept-blade air-flow angles, the following conclusions are indicated:

1. The blade-section pressure distributions indicate that, in order to obtain the same effective angle of attack on the swept-blade rotor as on the unswept-blade rotor, the blade twist should be increased by 3.8° for the entire radial span.

2. The induced effect of lift on angle of attack and twist due to sweep was partially offset by the blockage of the blade; for the swept blade, this reduction in area decreased the required increase in twist by an estimated 50 percent.

3. Two-dimensional cascade data were adequate in predicting the blade turning angle at the trailing edge of the swept blade. In order to obtain the turning angle at any station farther downstream, the change in axial velocity due to the trailing portion of the blade must be taken into account.

Langley Aeronautical Laboratory,
National Advisory Committee for Aeronautics,
Langley Field, Va., April 29, 1957.

REFERENCES

1. Westphal, Willard R., and Godwin, William R.: Comparison of NACA 65-Series Compressor-Blade Pressure Distributions and Performance in a Rotor and in Cascade. NACA TN 3806, 1957. (Supersedes NACA RM L51H20.)
2. Schulze, Wallace M., Ashby, George C., Jr., and Erwin, John R.: Several Combination Probes for Surveying Static and Total Pressure and Flow Direction. NACA TN 2830, 1952.
3. DeYoung, John, and Harper, Charles W.: Theoretical Symmetric Span Loading at Subsonic Speeds for Wings Having Arbitrary Plan Form. NACA Rep. 921, 1948.
4. Felix, A. Richard: Summary of 65-Series Compressor-Blade Low-Speed Cascade Data by Use of the Carpet-Plotting Technique. NACA TN 3913, 1957. (Supersedes NACA RM L54H18a.)

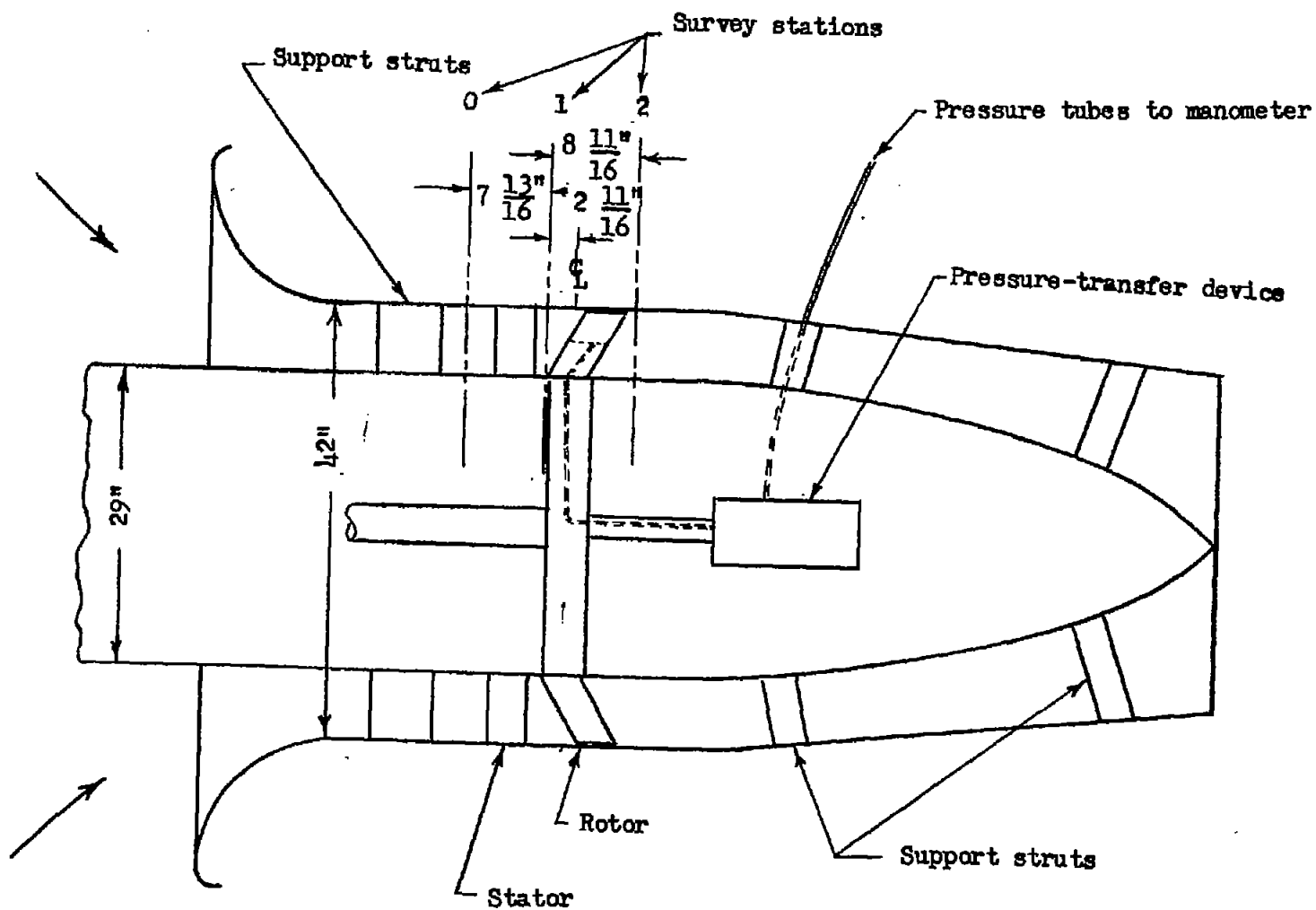


Figure 1.- Schematic sketch of test section.

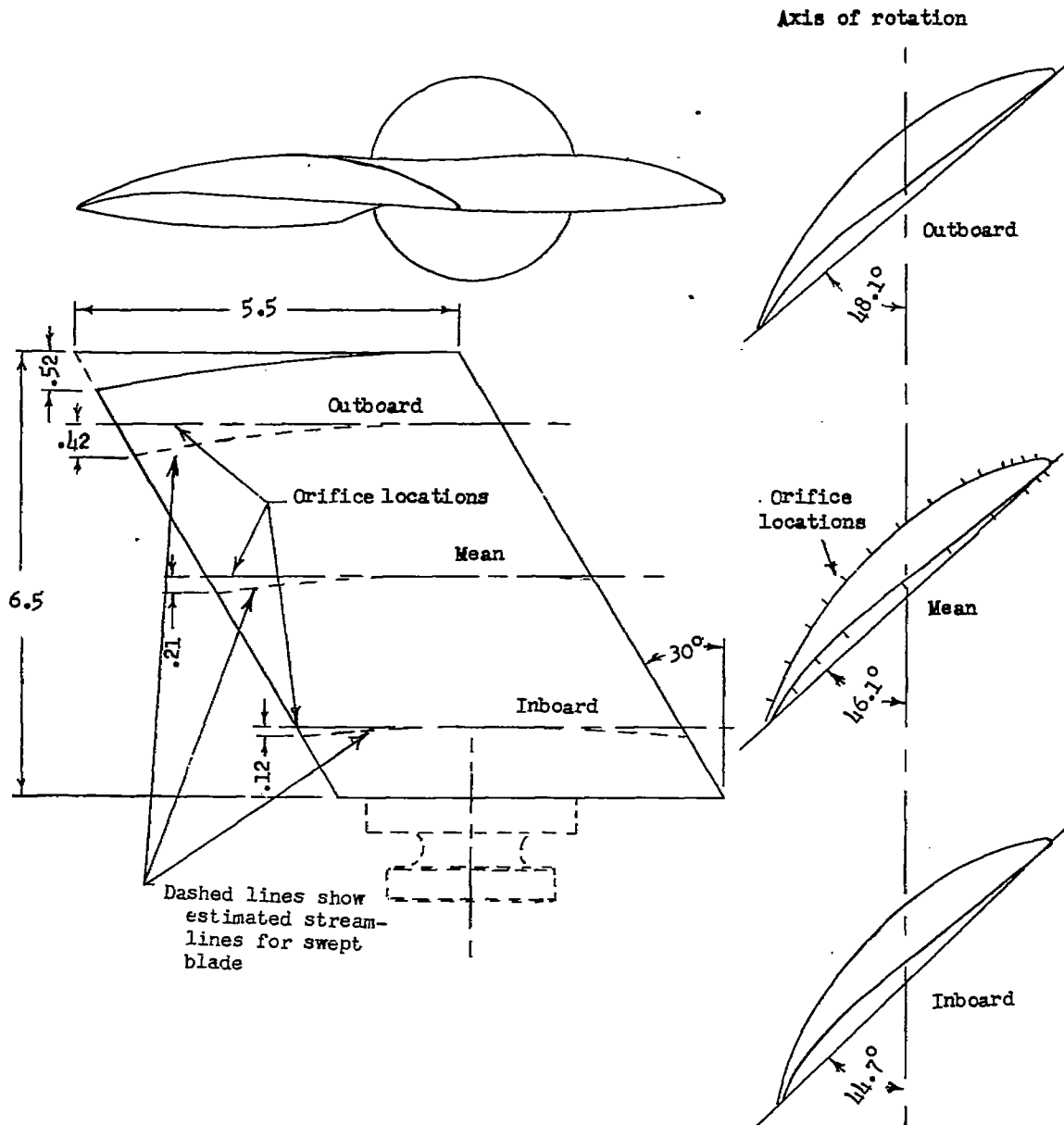


Figure 2.- Sketch of rotor blade. Linear dimensions are in inches.

| | β_1 , deg | $\beta_{1,r}$, deg | α , deg | θ , deg |
|----------|-----------------|---------------------|----------------|----------------|
| Outboard | 36.4 | 60.0 | 11.9 | 15.1 |
| Mean | 41.1 | 59.7 | 13.6 | 19.7 |
| Inboard | 46.9 | 60.2 | 15.5 | 25.6 |

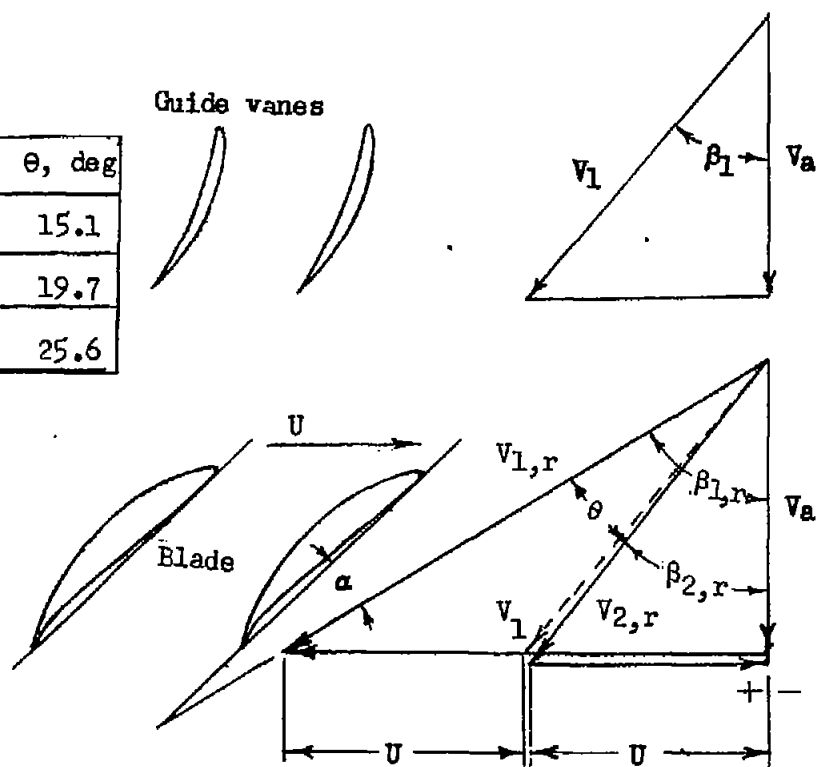
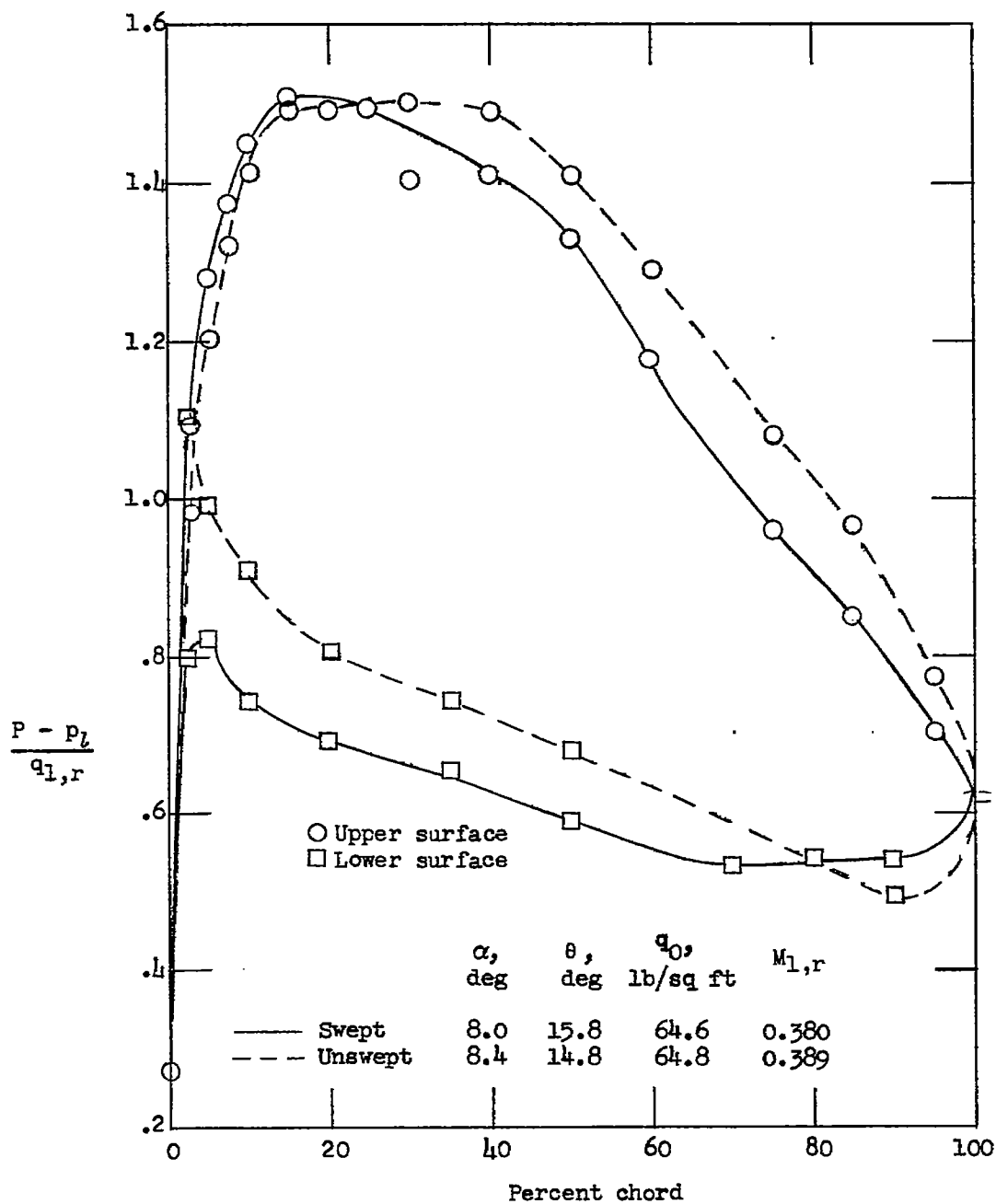
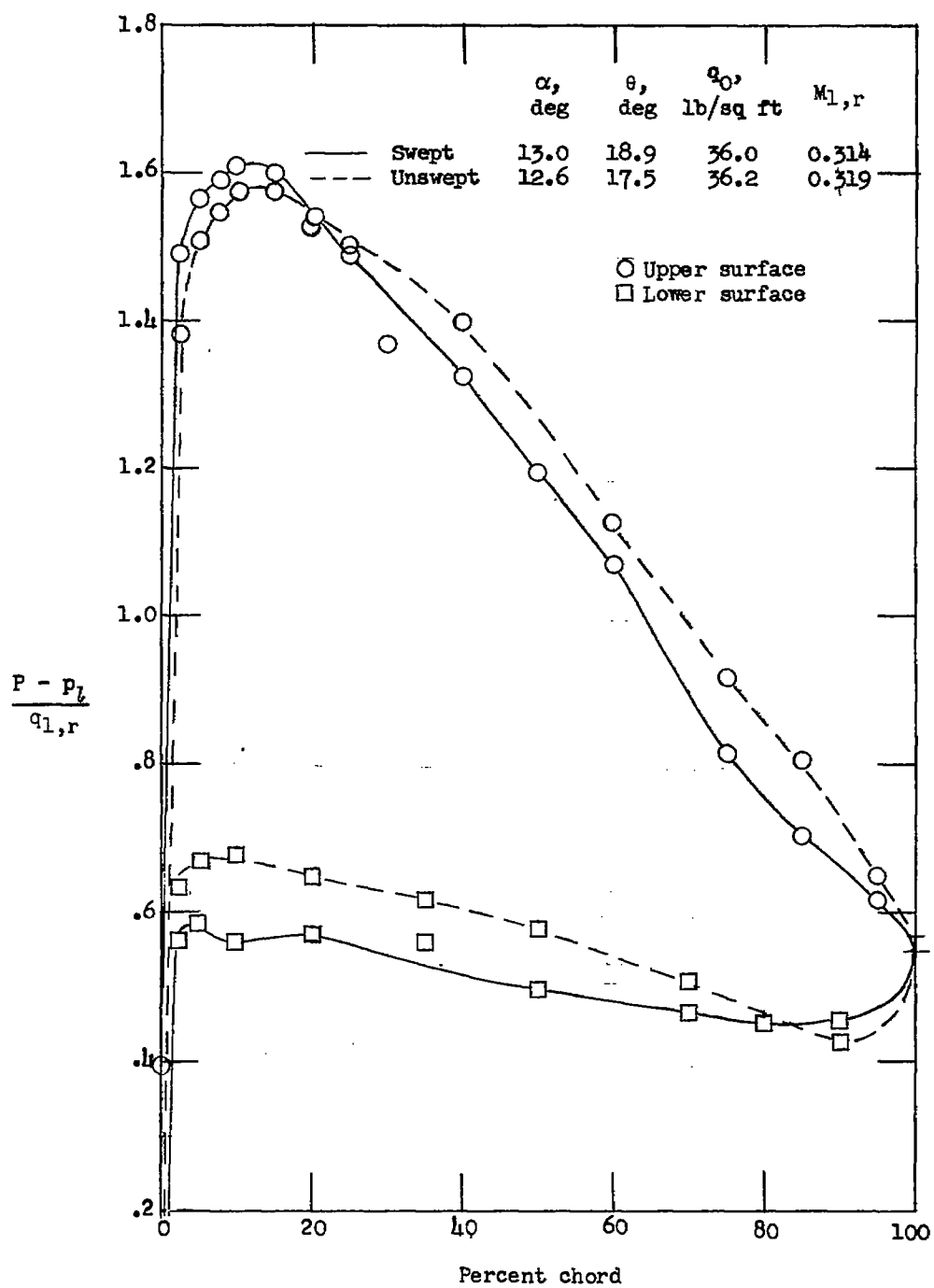


Figure 3.- Velocity diagram at design conditions.



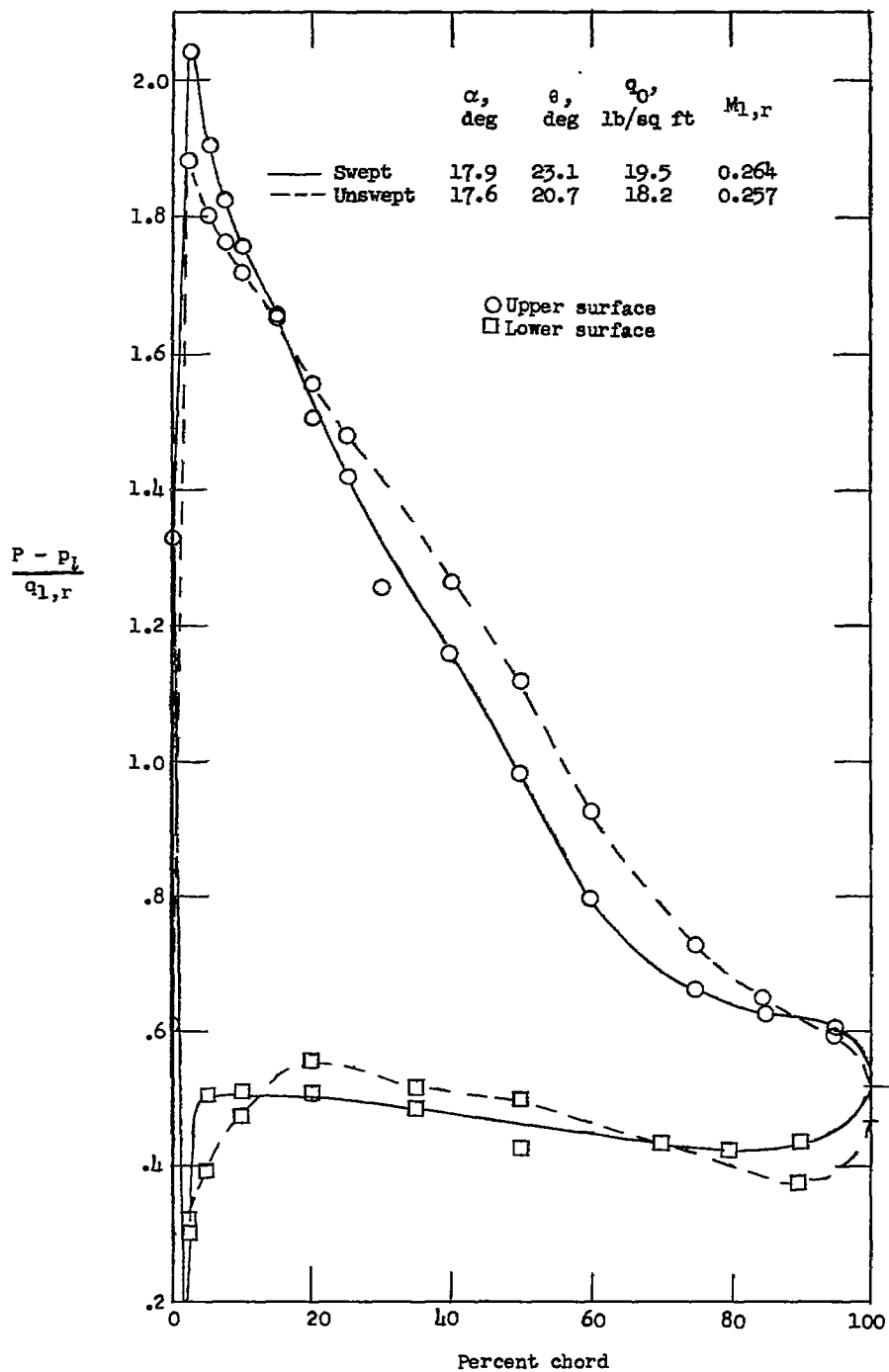
(a) Open-throttle condition.

Figure 4.- Comparison of pressure distributions for the swept and unswept blades at the outboard section.



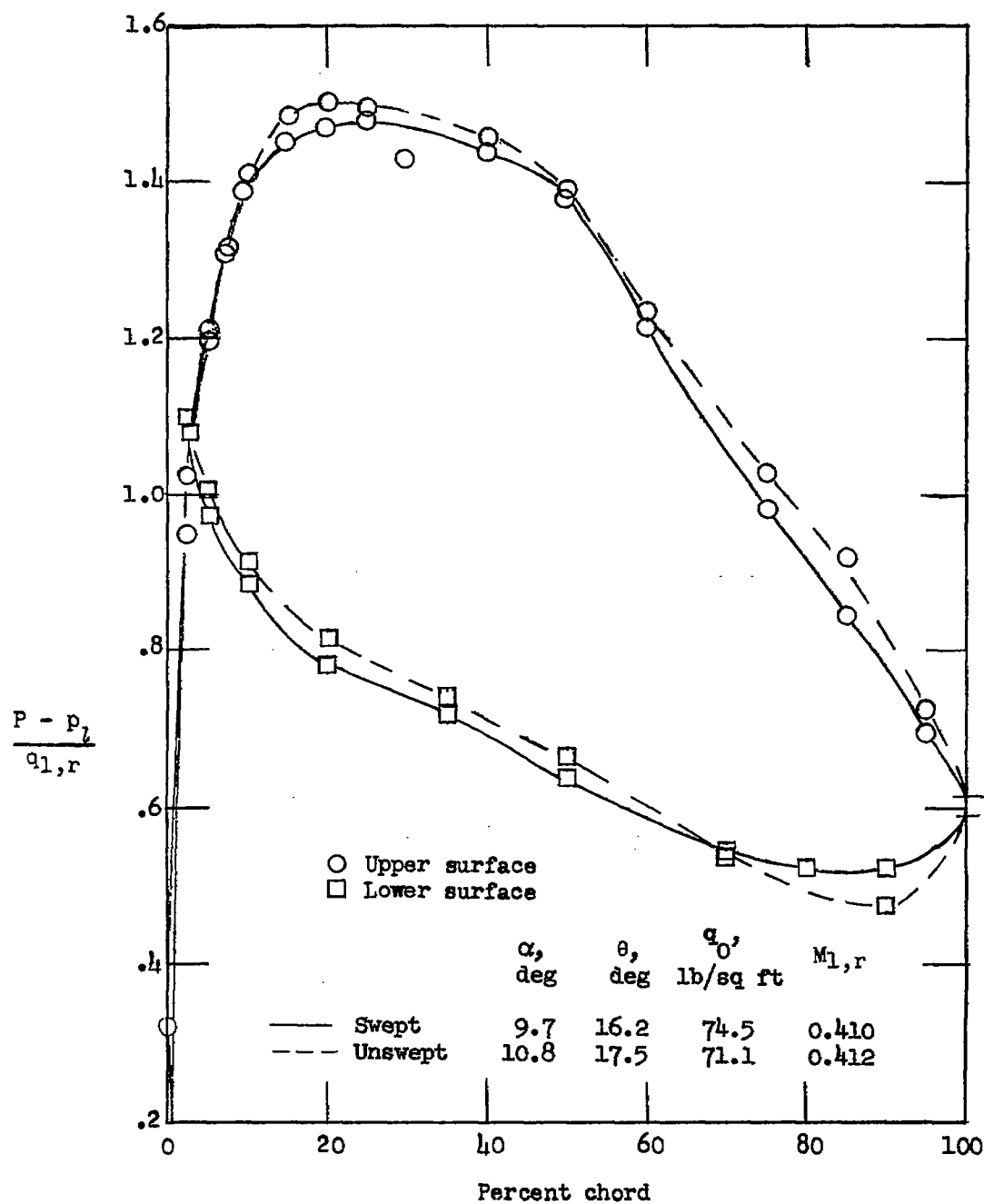
(b) Design condition.

Figure 4.- Continued.



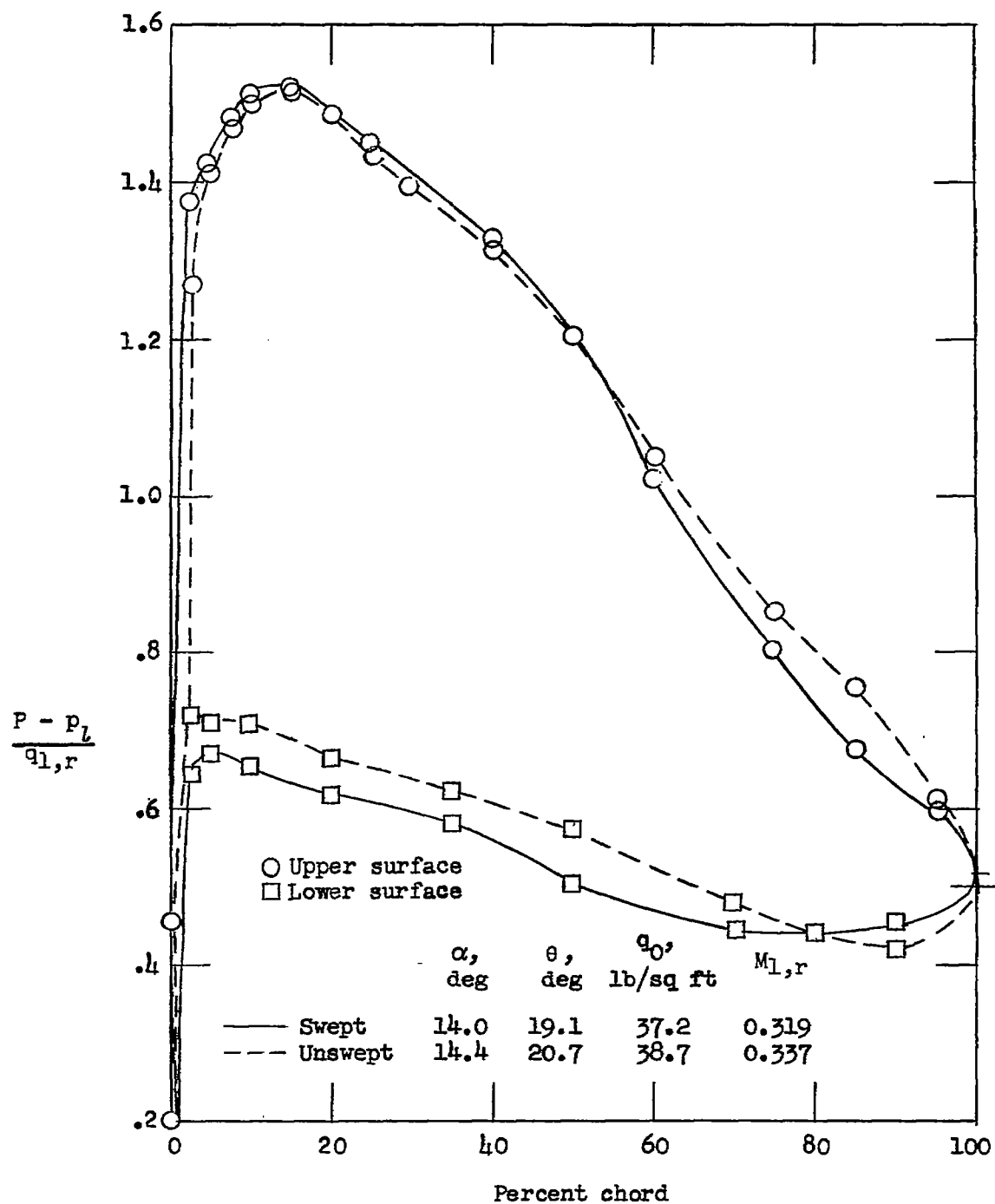
(c) Near-surge condition.

Figure 4.- Concluded.



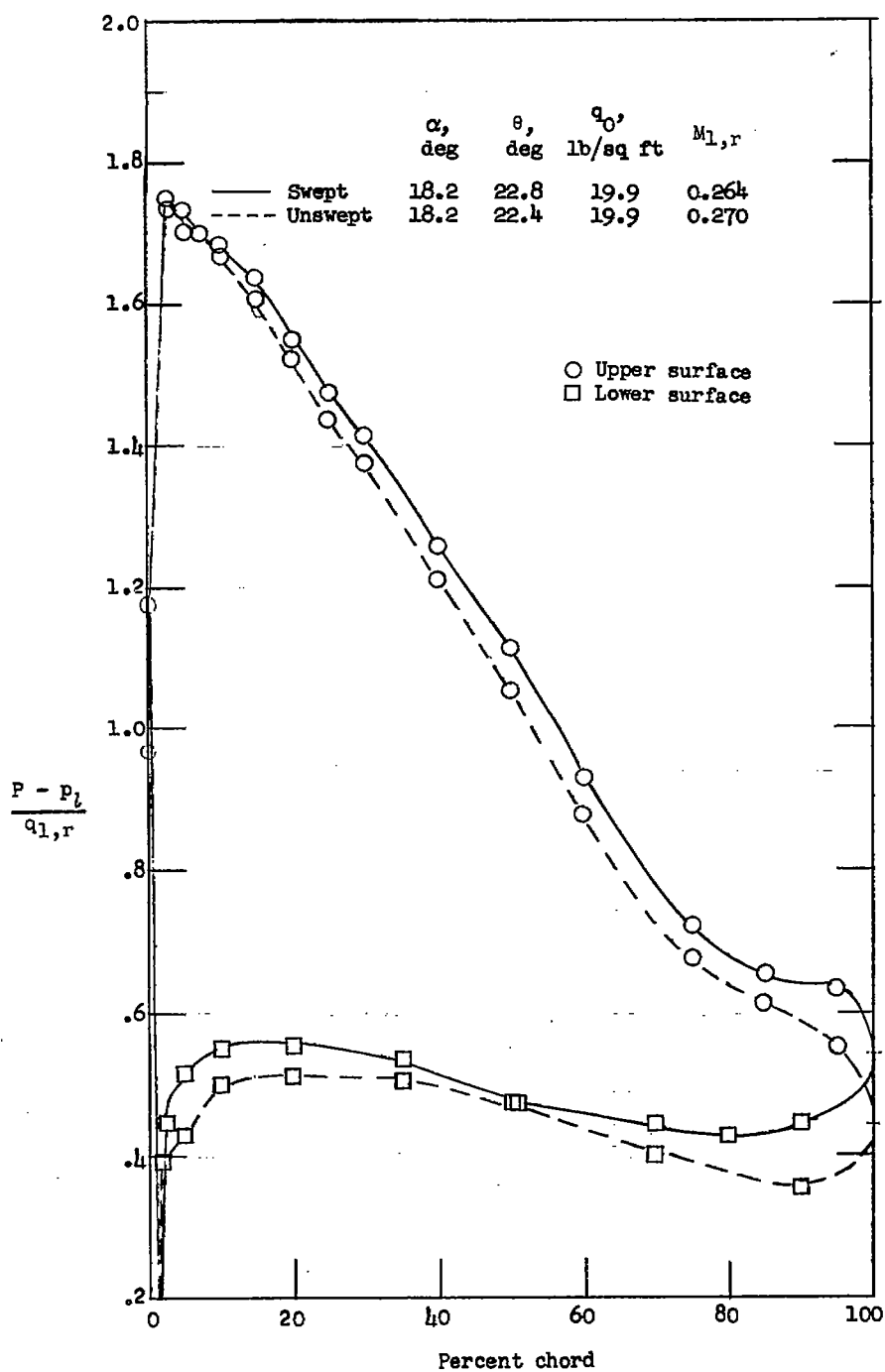
(a) Open-throttle condition.

Figure 5.- Comparison of pressure distributions for the swept and unswept blades at the mean section.



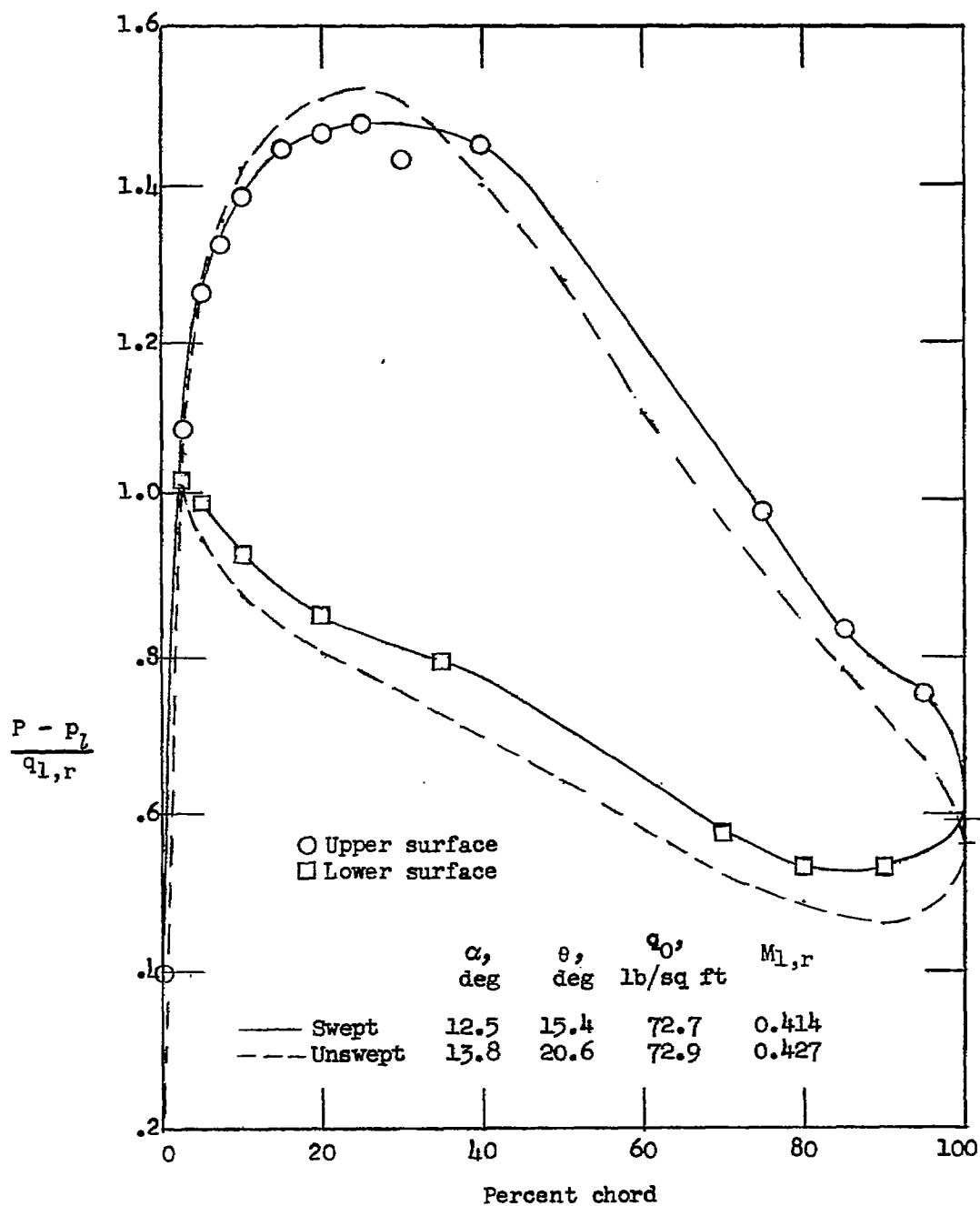
(b) Design condition.

Figure 5.- Continued.



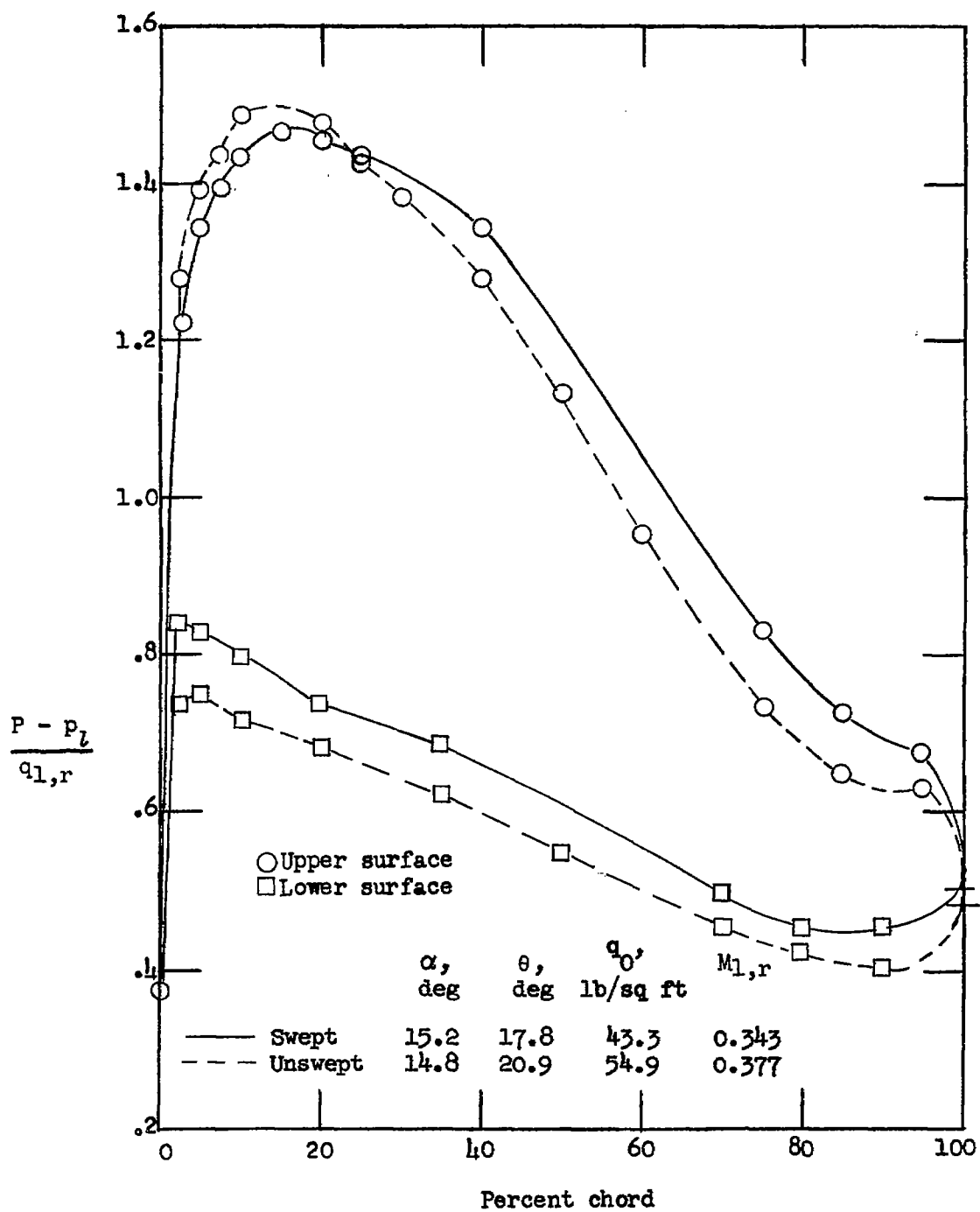
(c) Near-surge condition.

Figure 5.- Concluded.



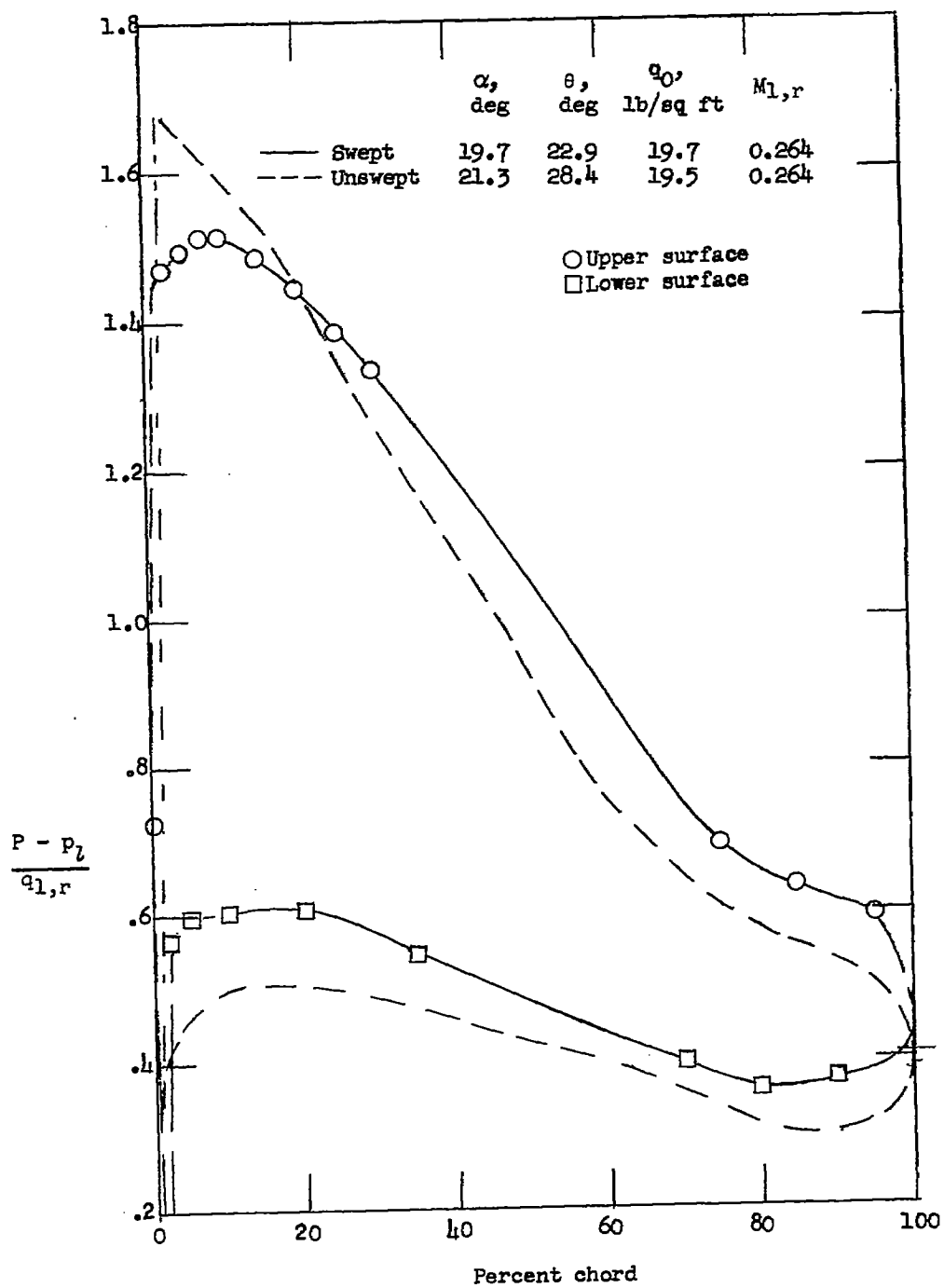
(a) Open-throttle condition.

Figure 6.- Comparison of pressure distributions for the swept and unswept blades at the inboard section.



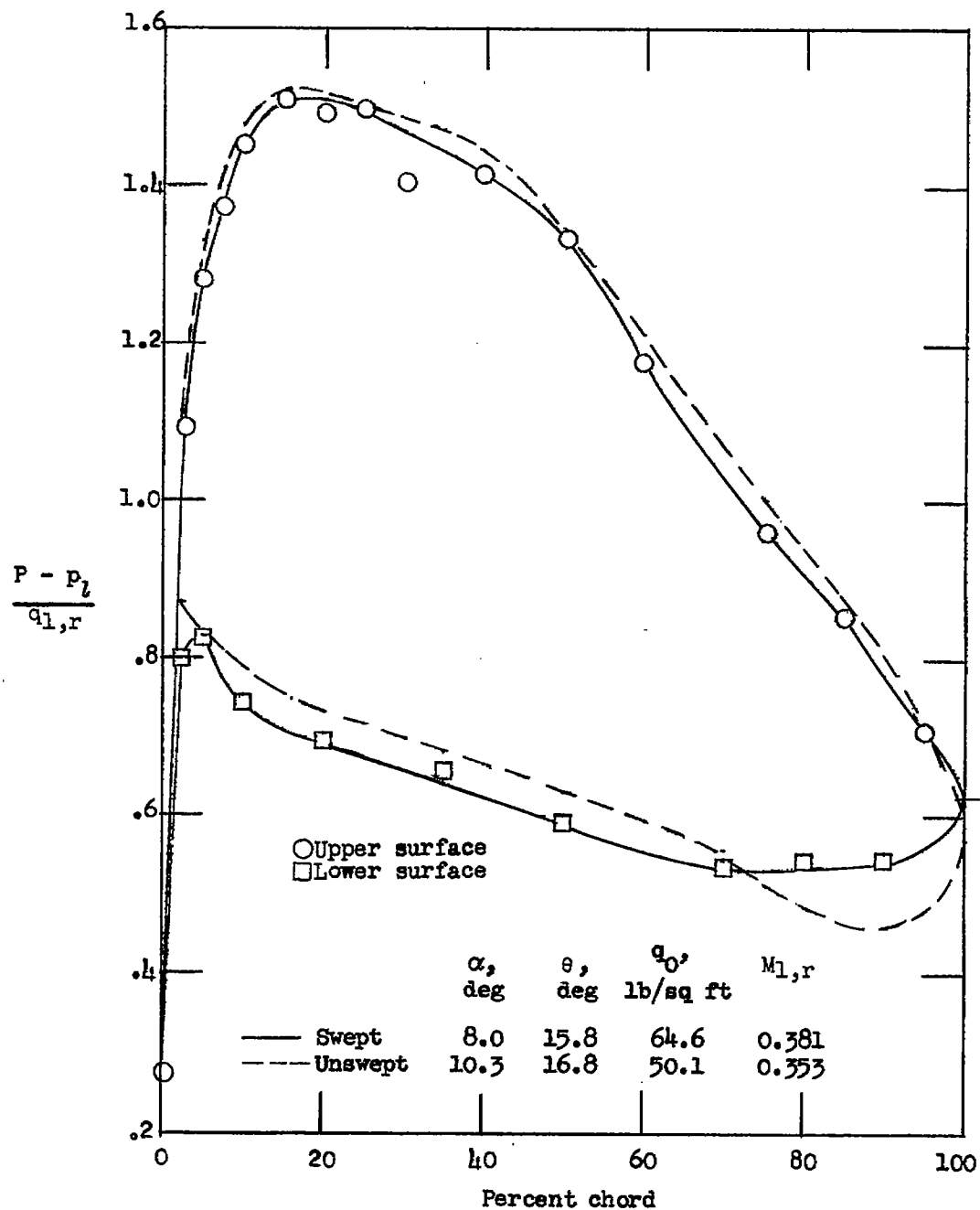
(b) Design condition.

Figure 6.- Continued.



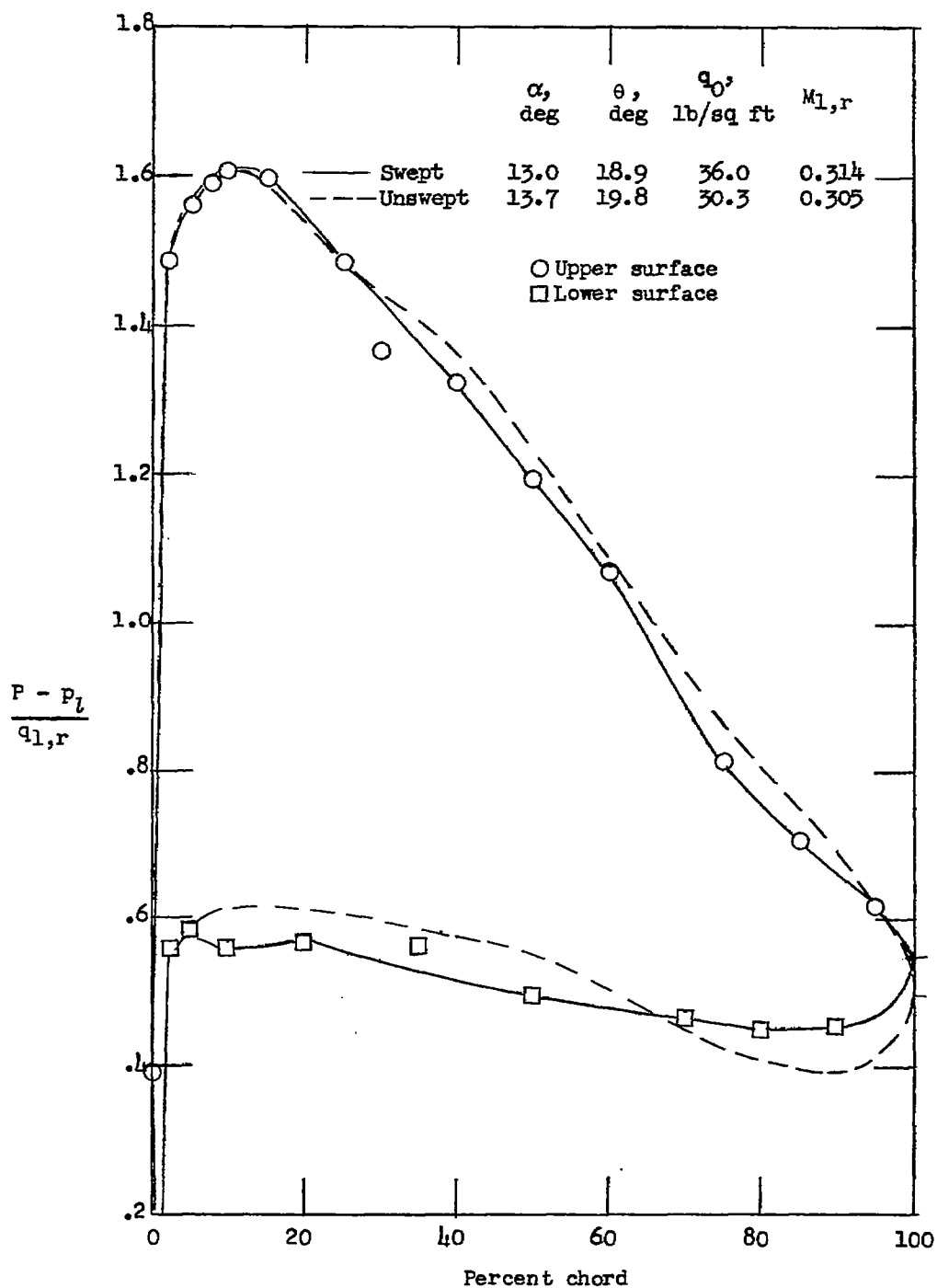
(c) Near-surge condition.

Figure 6.- Concluded.



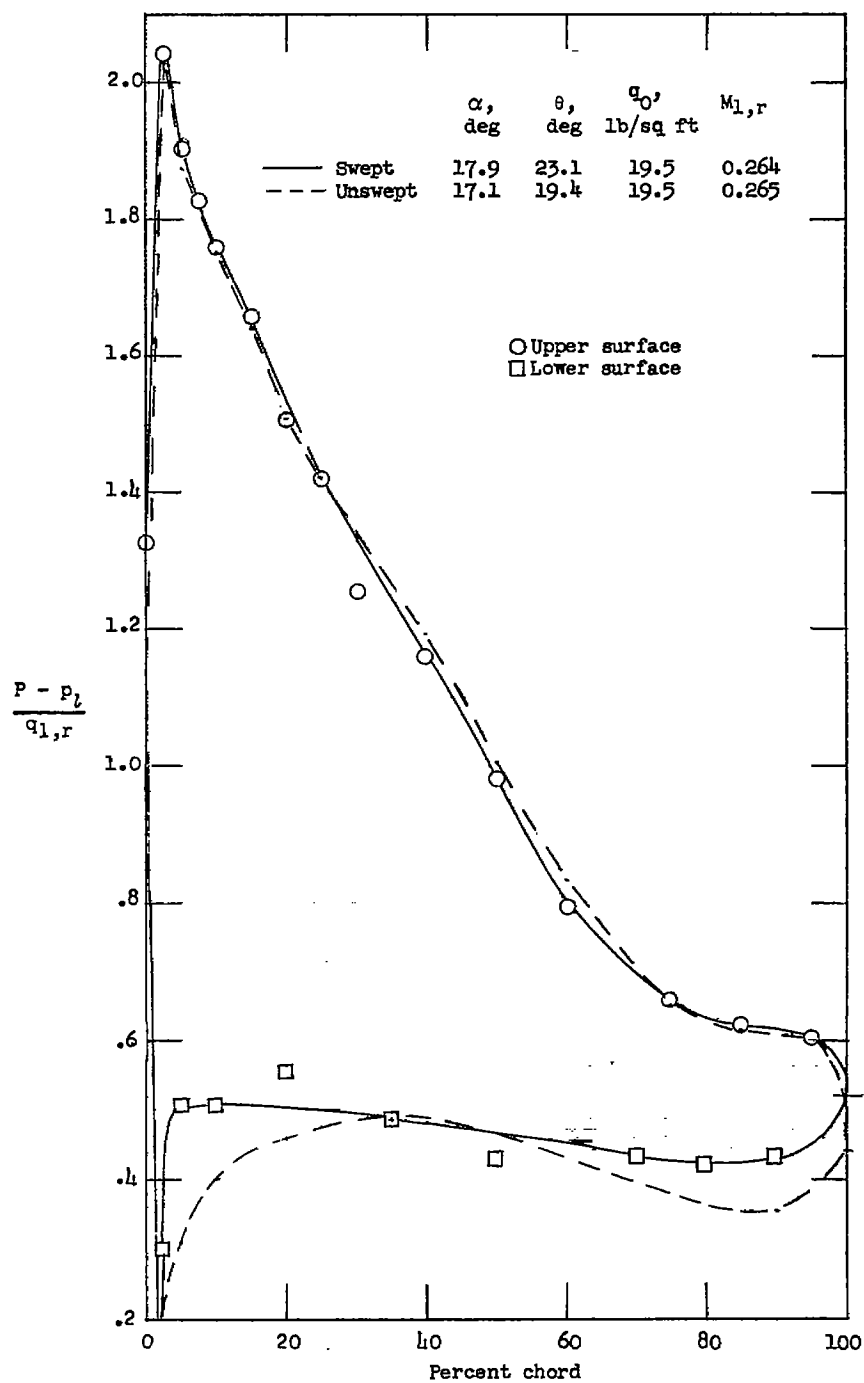
(a) Open-throttle condition.

Figure 7.- Similar pressure distributions for the swept and unswept blades at the outboard section.



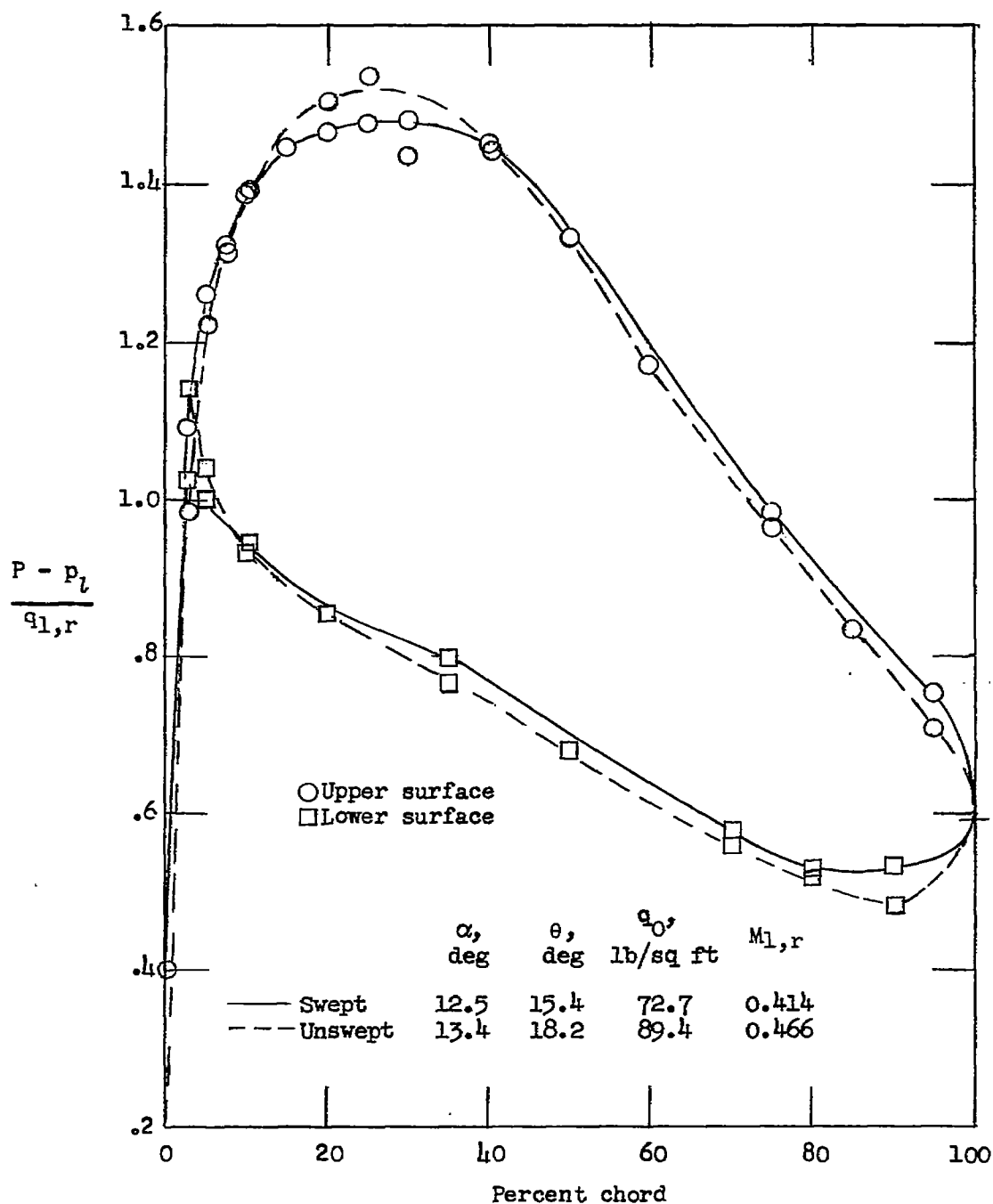
(b) Design condition.

Figure 7.- Continued.



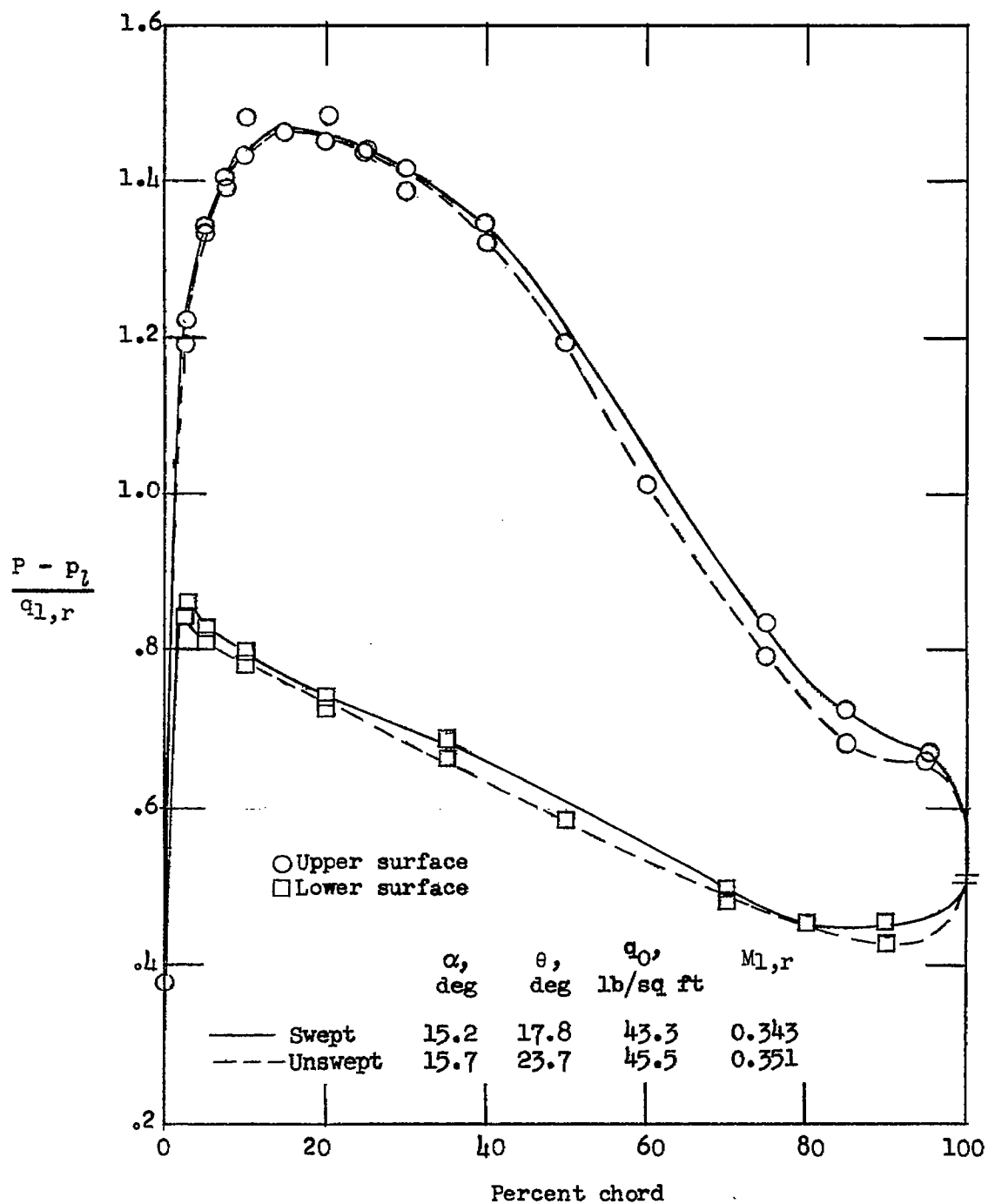
(c) Near-surge condition.

Figure 7.- Concluded.



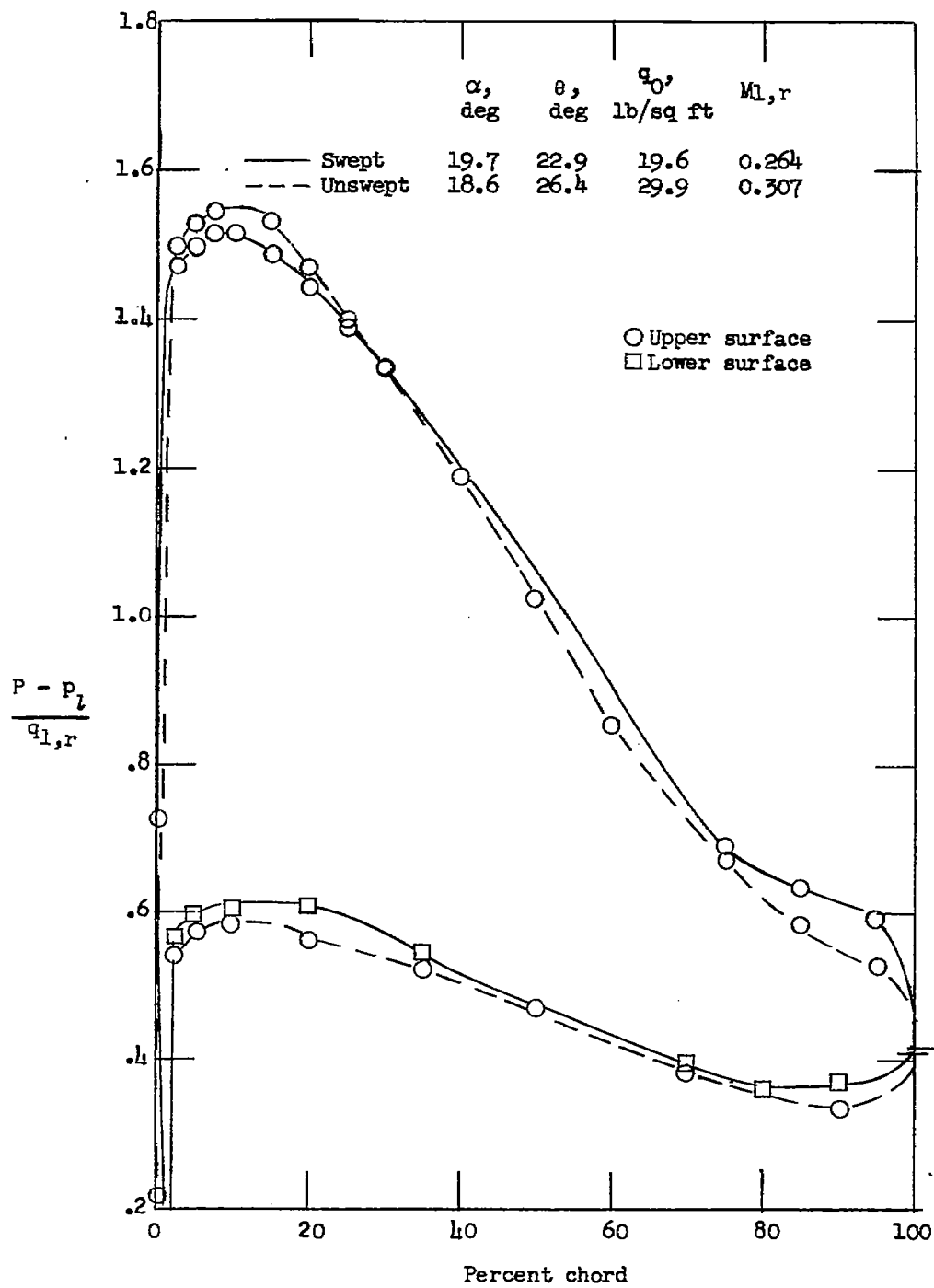
(a) Open-throttle condition.

Figure 8.- Similar pressure distributions for the swept and unswept blades at the inboard section.



(b) Design condition.

Figure 8.- Continued.



(c) Near-surge condition.

Figure 8.- Concluded.

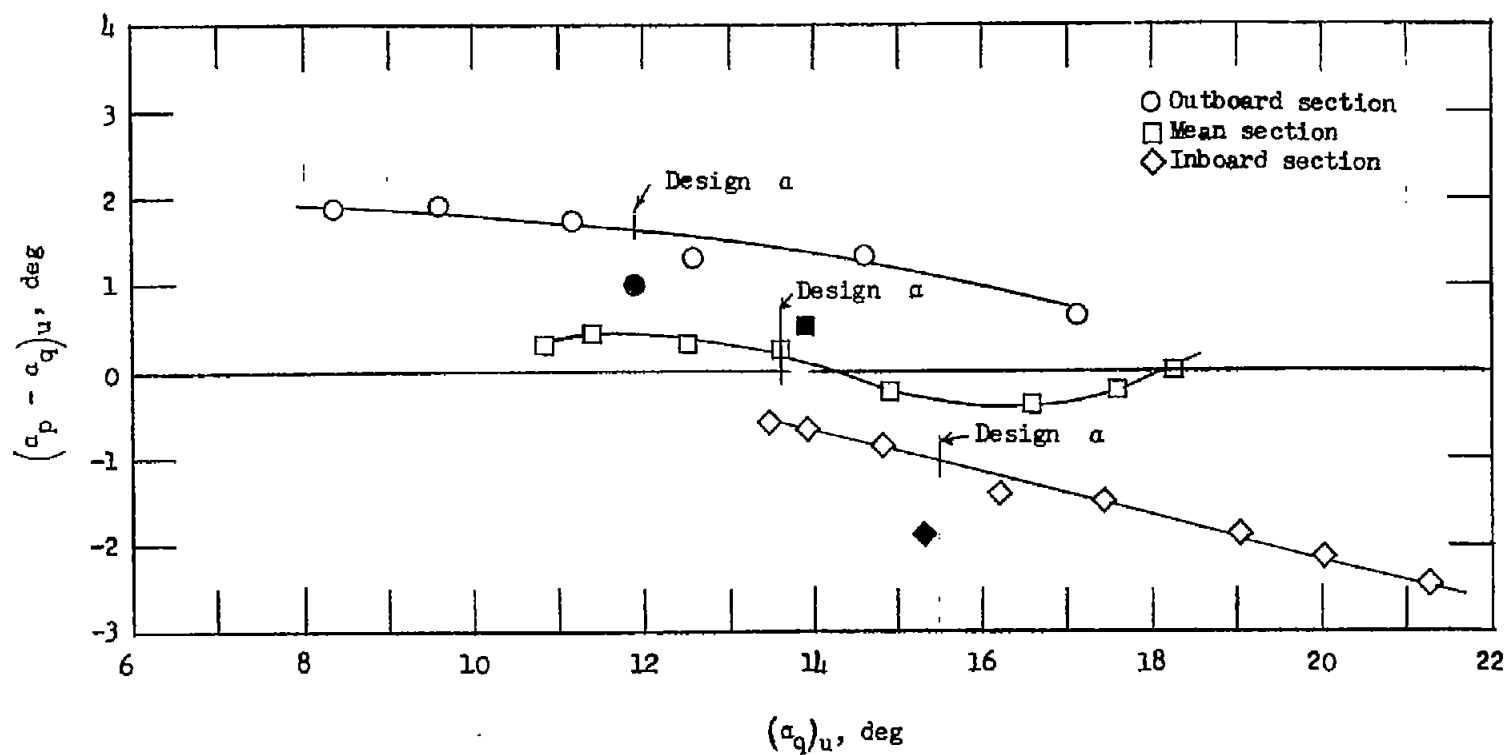


Figure 9.- Change in effective angle of attack of the blade sections due to 30° sweep. The shaded symbols denote predicted values of twist for the design condition for an isolated airfoil estimated from the charts of reference 3.

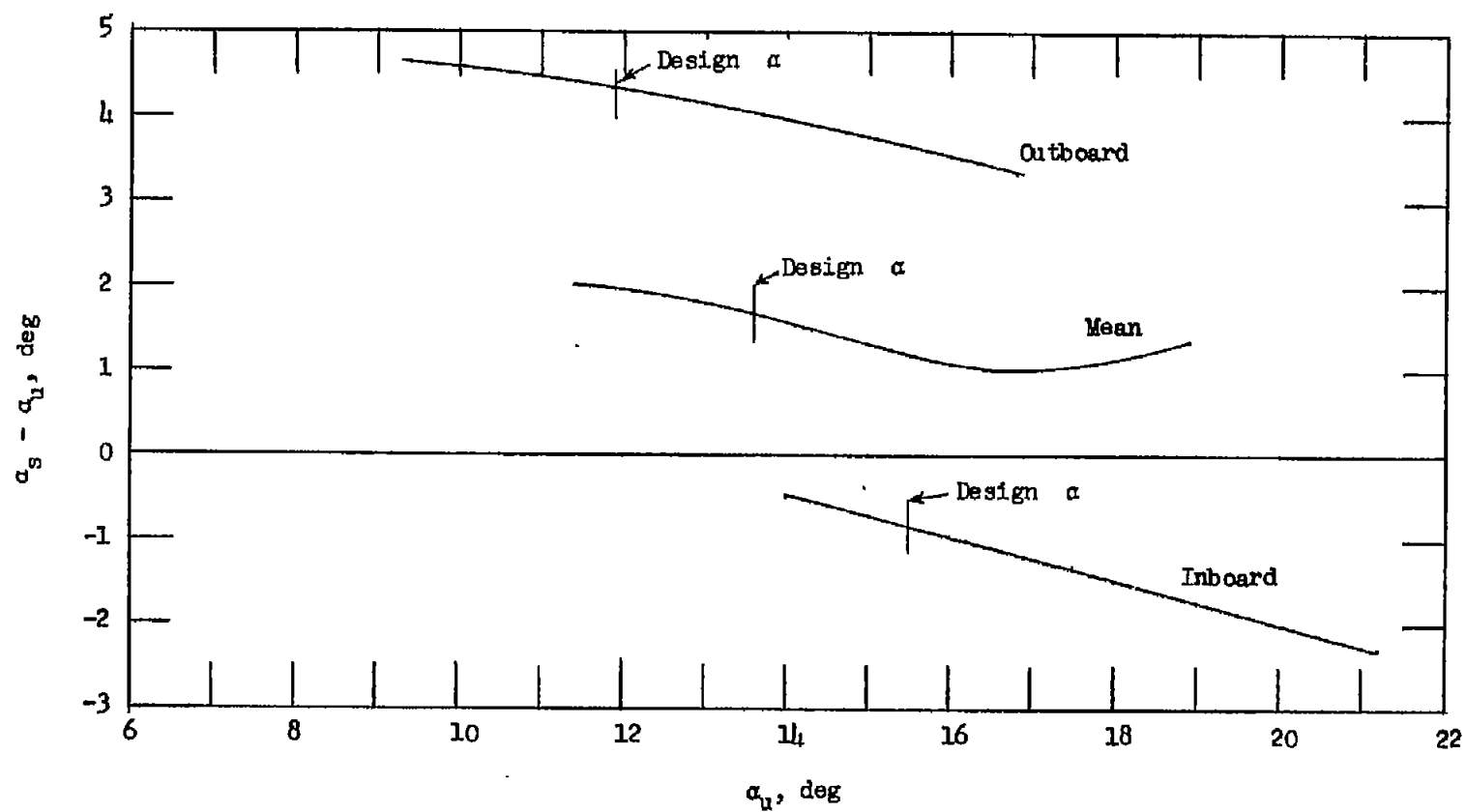
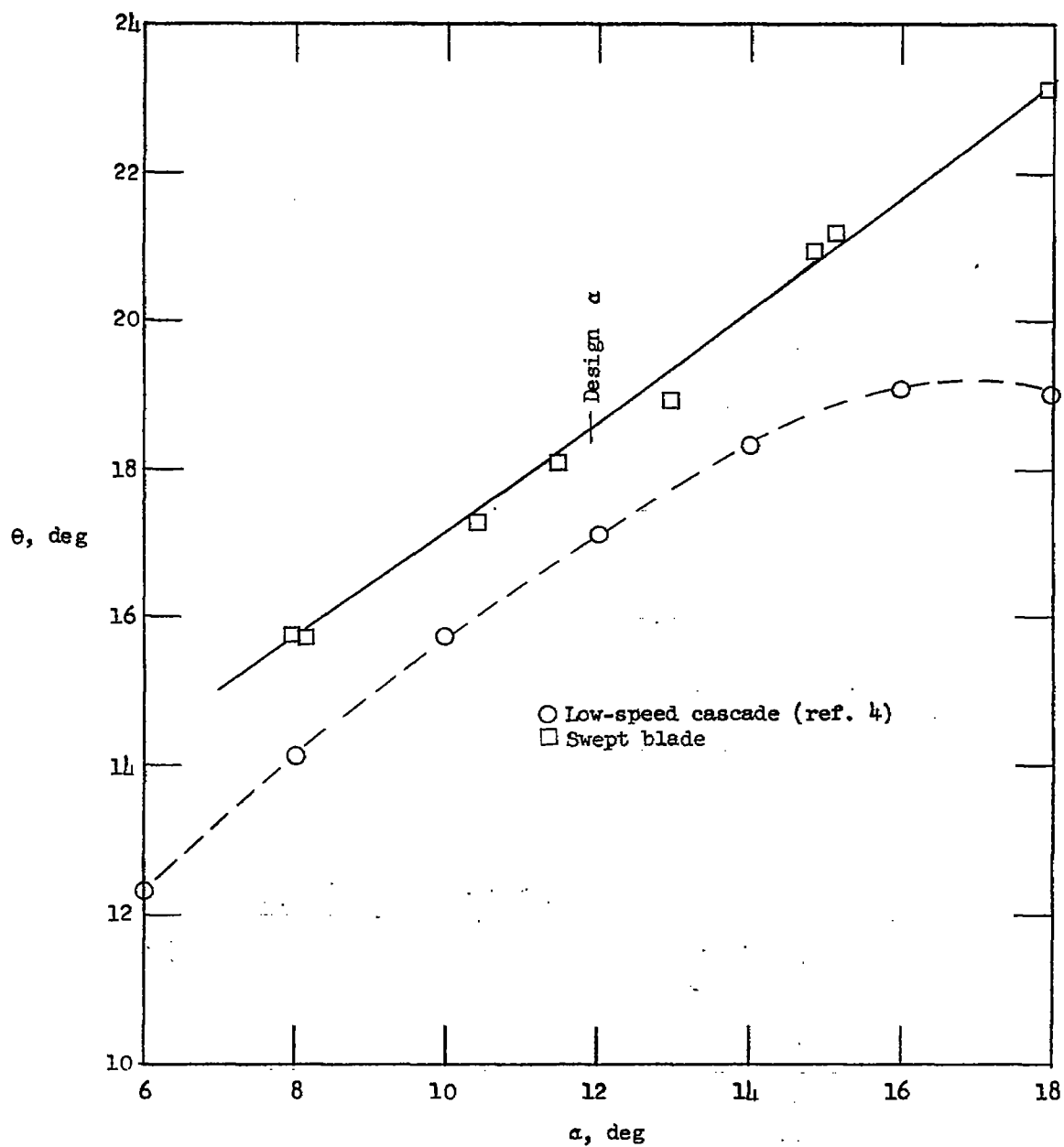
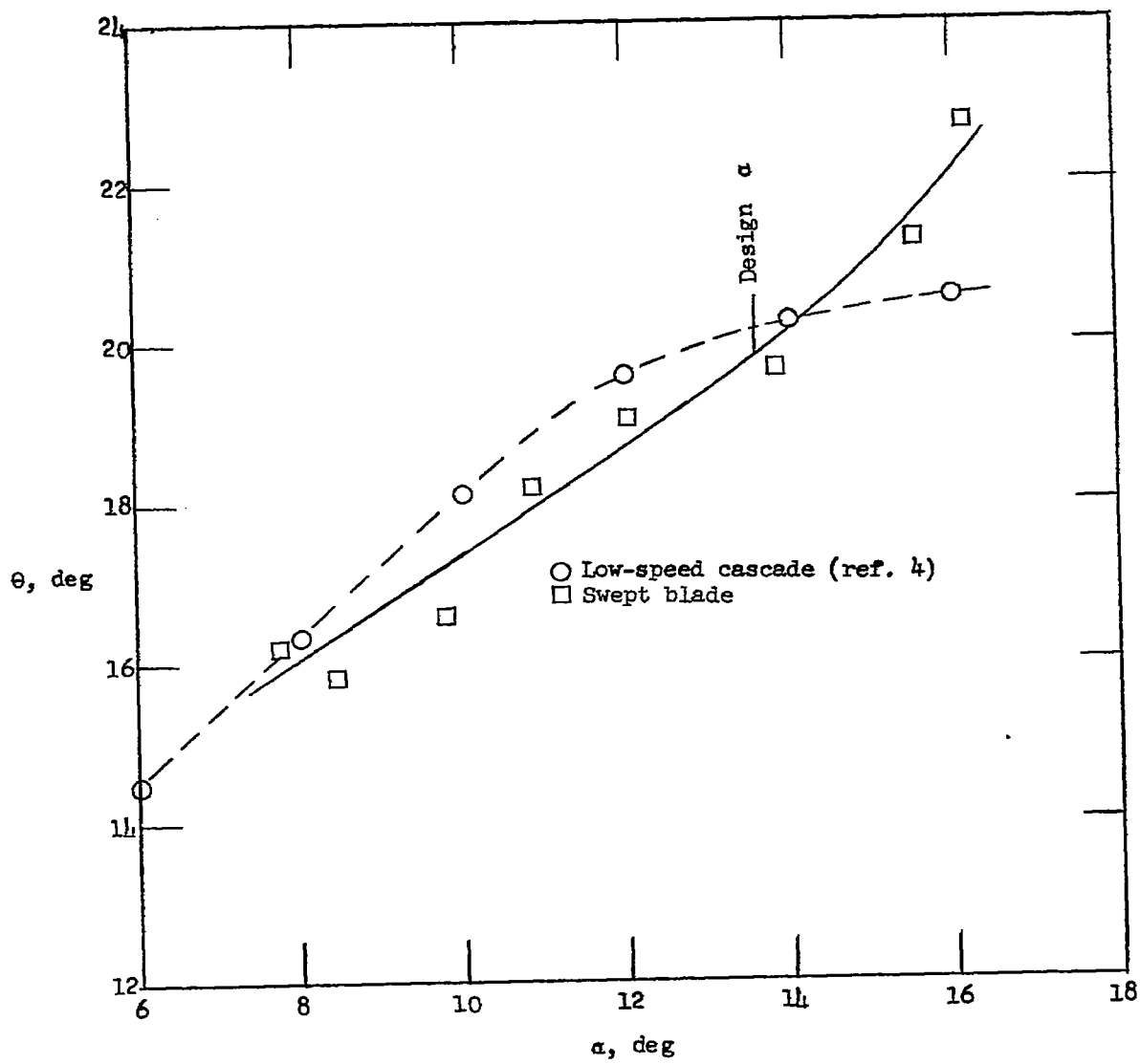


Figure 10.- Estimated change in effective angle of attack due to 30° sweep without blade thickness effect.



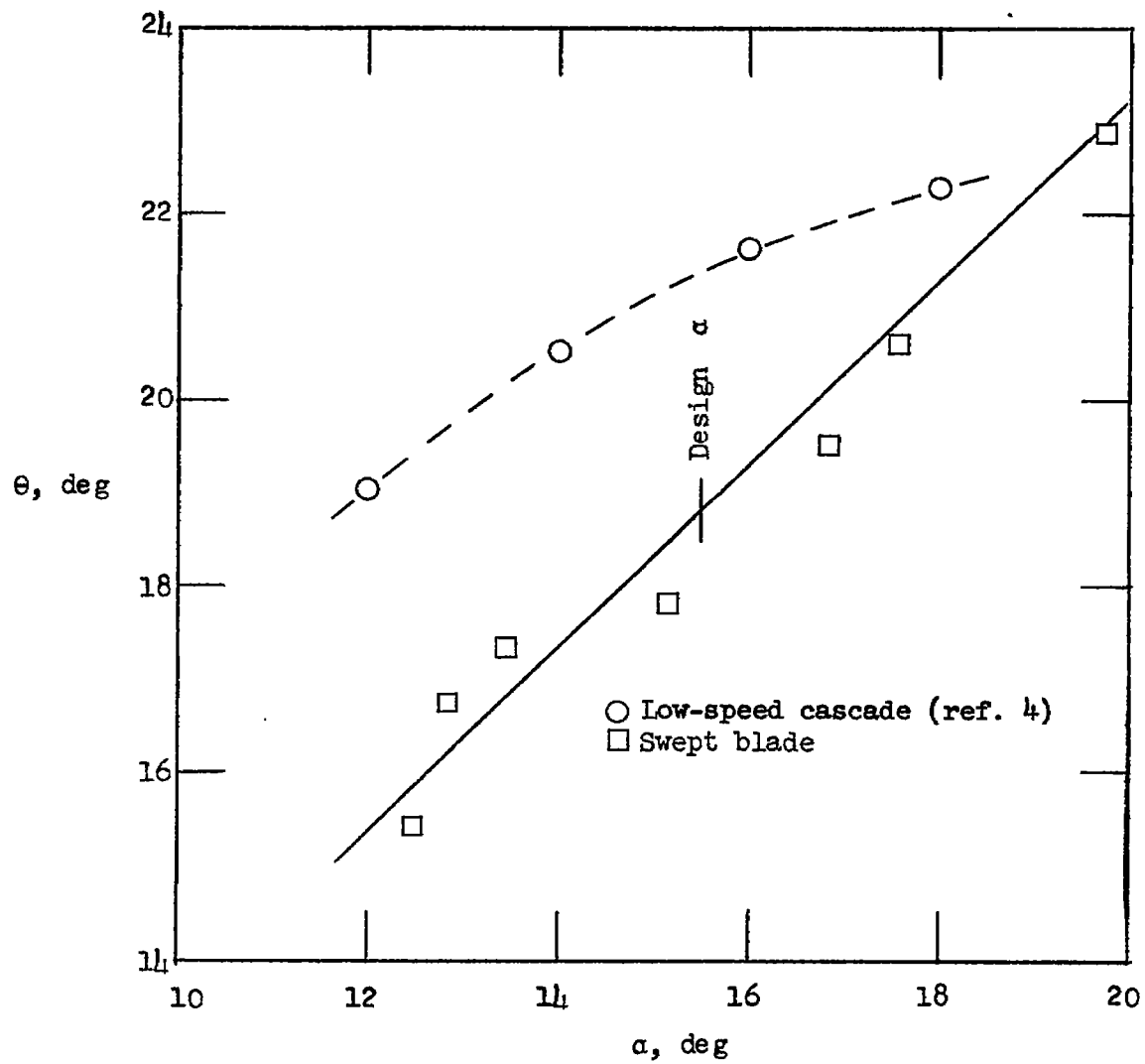
(a) Outboard section.

Figure 11.- Turning angle against angle of attack.



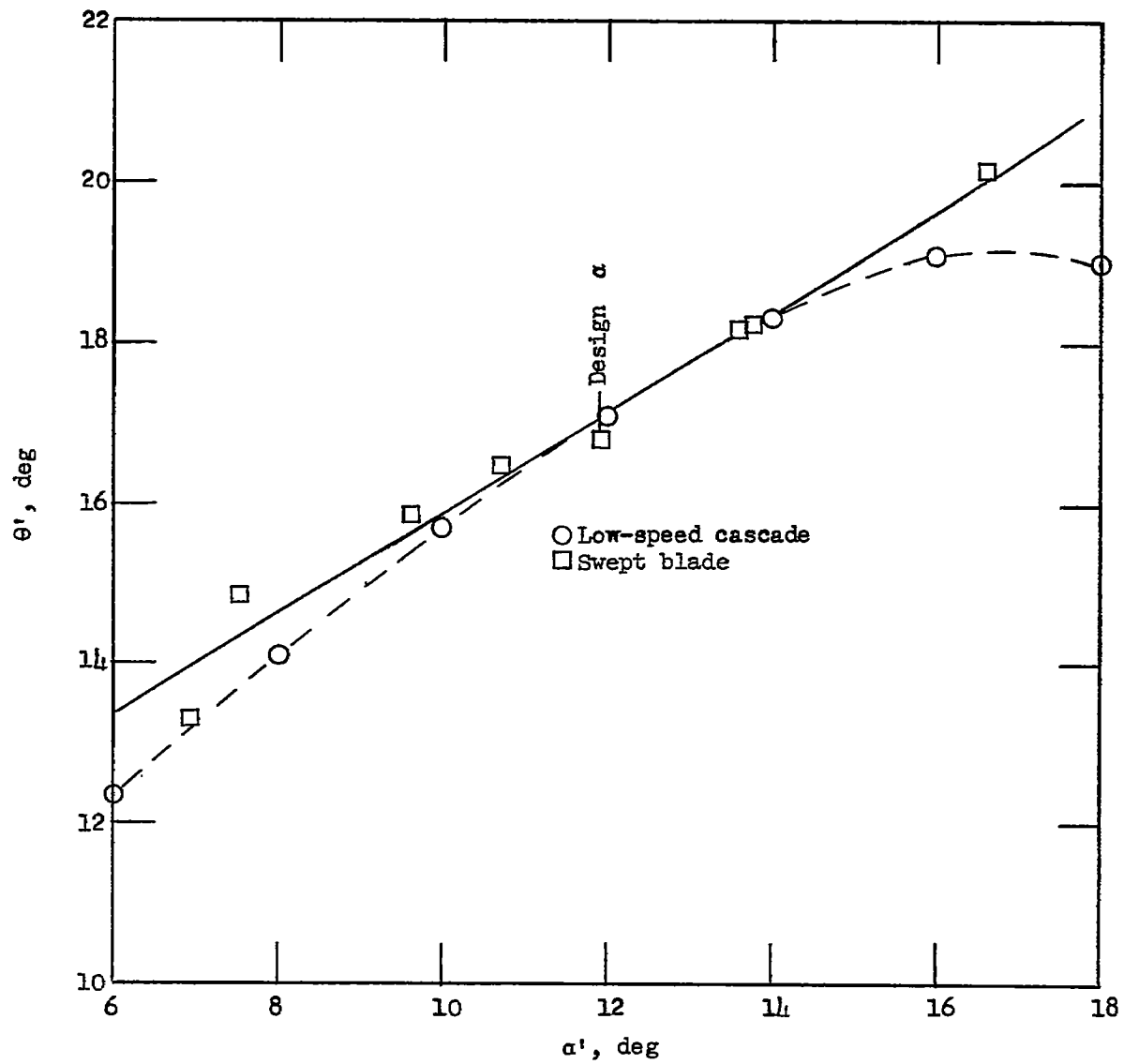
(b) Mean section.

Figure 11.- Continued.



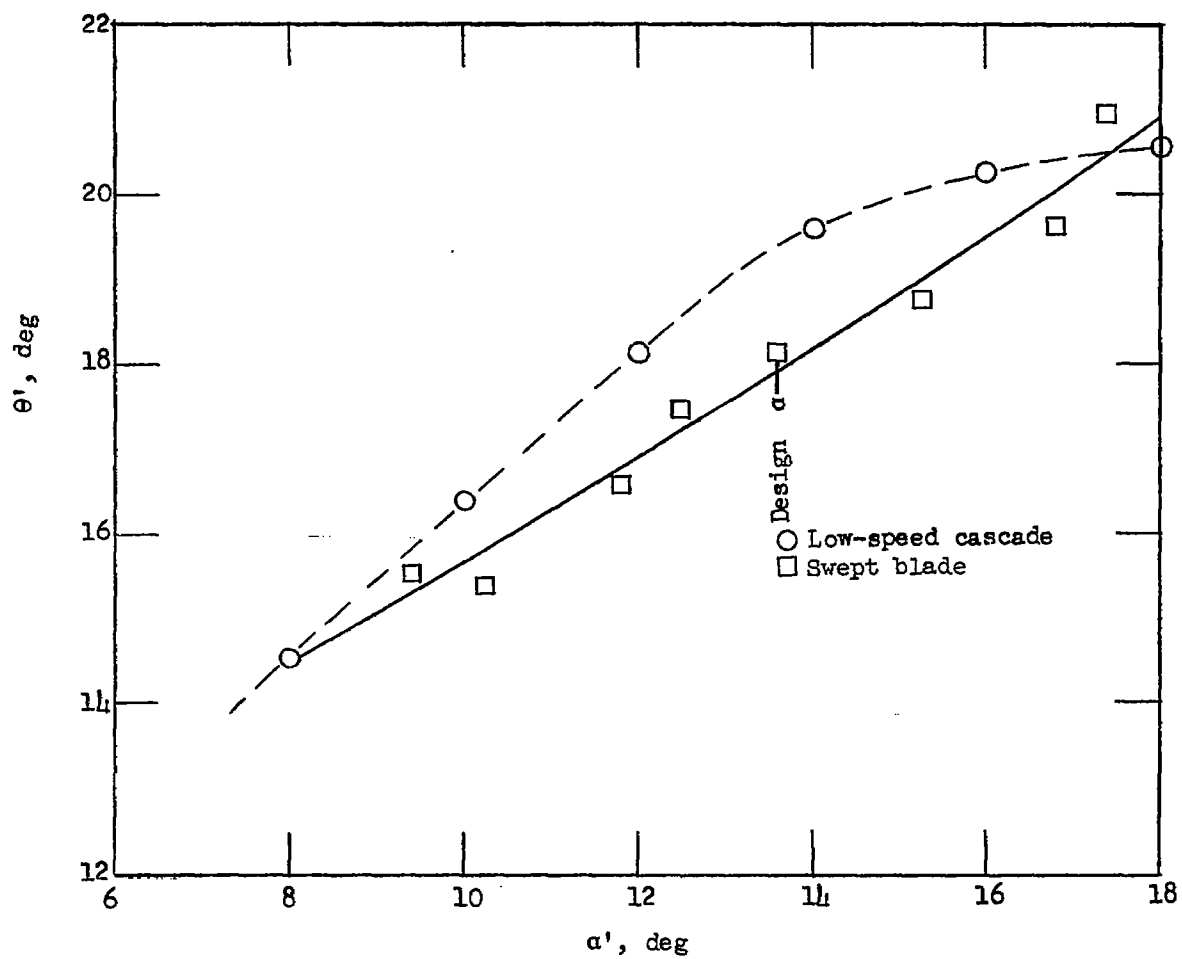
(c) Inboard section.

Figure 11.- Concluded.



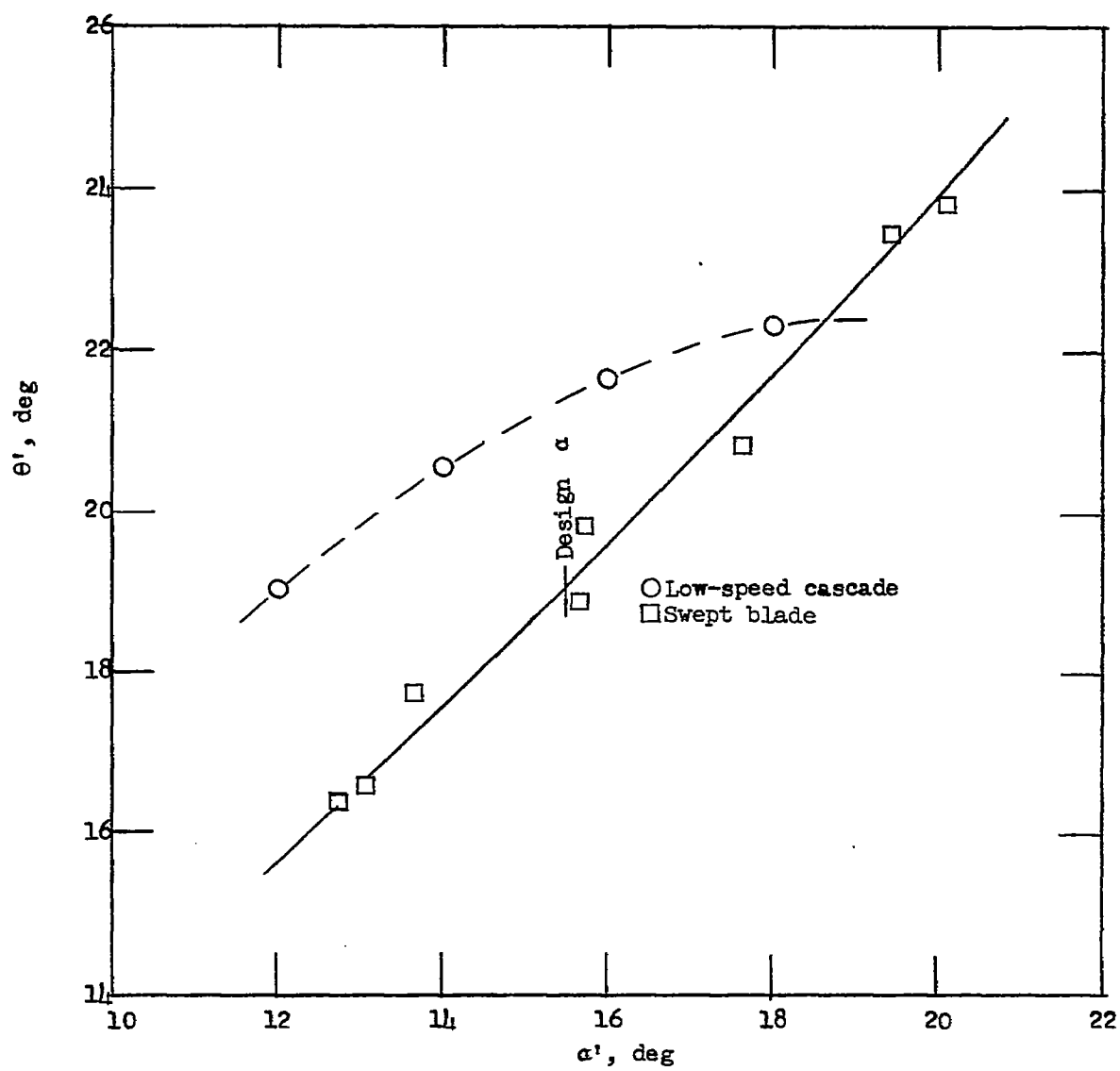
(a) Outboard section.

Figure 12.- Turning angle against angle of attack, corrected to a mean axial velocity.



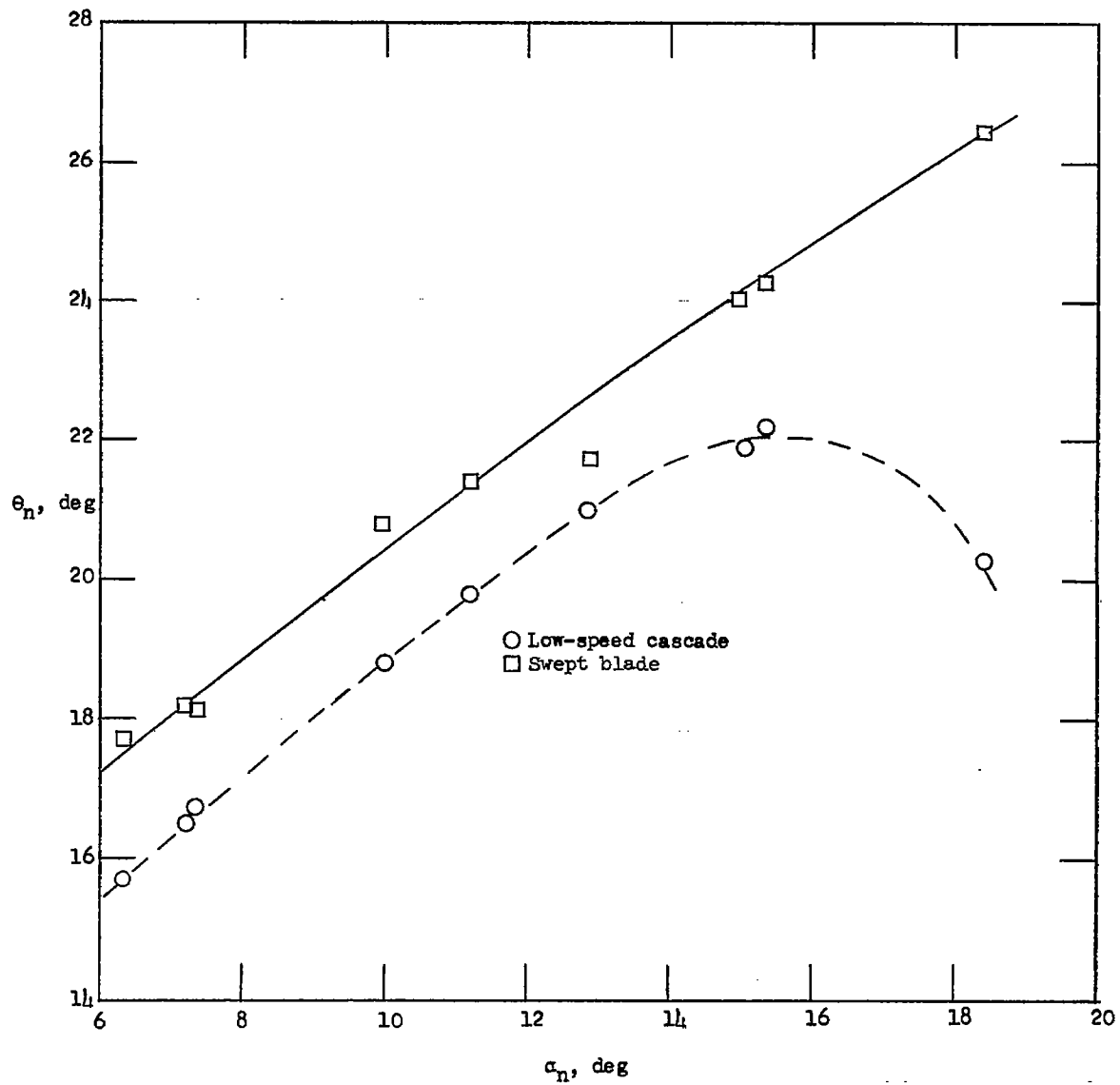
(b) Mean section.

Figure 12.- Continued.



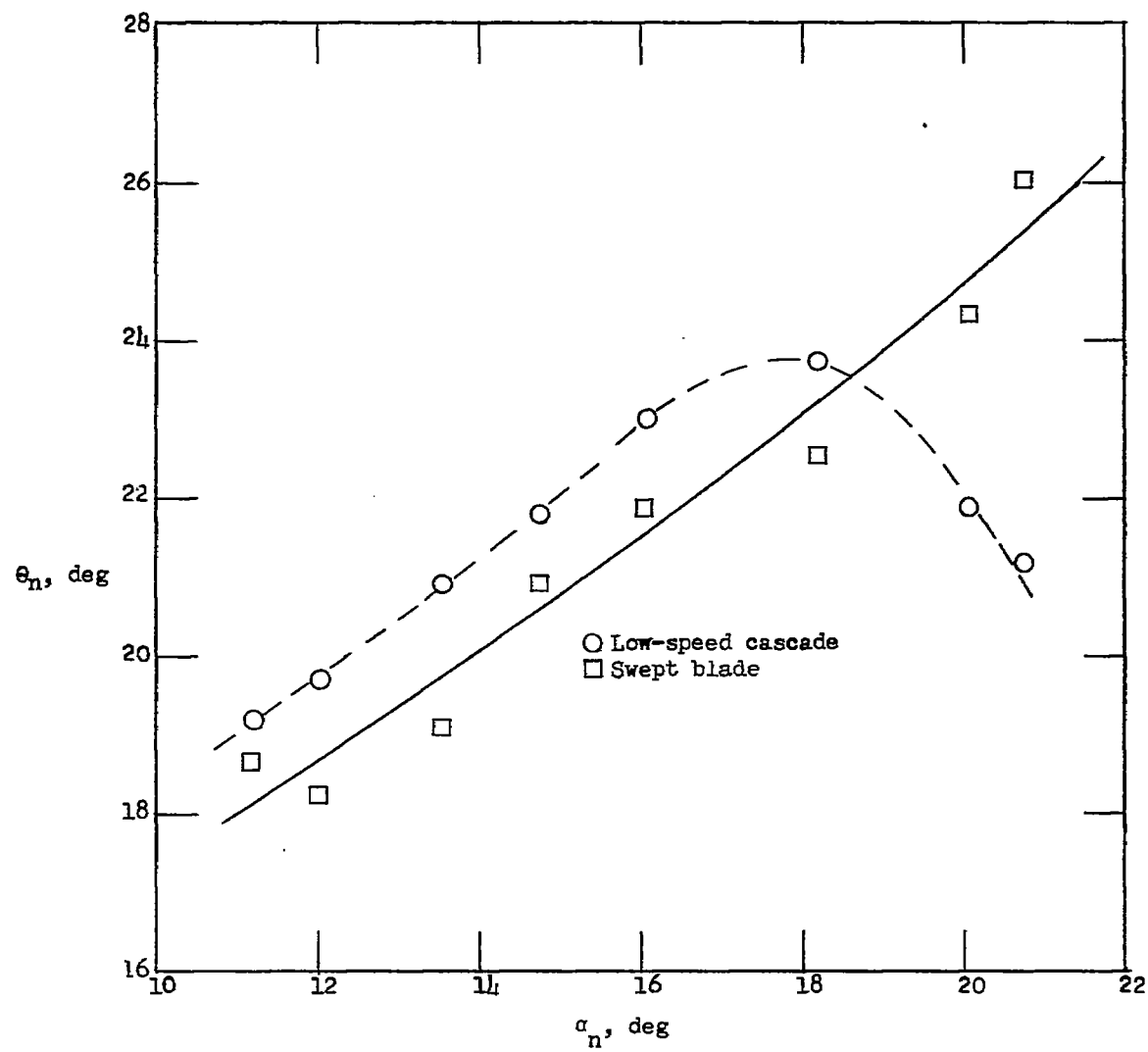
(c) Inboard section.

Figure 12.- Concluded.



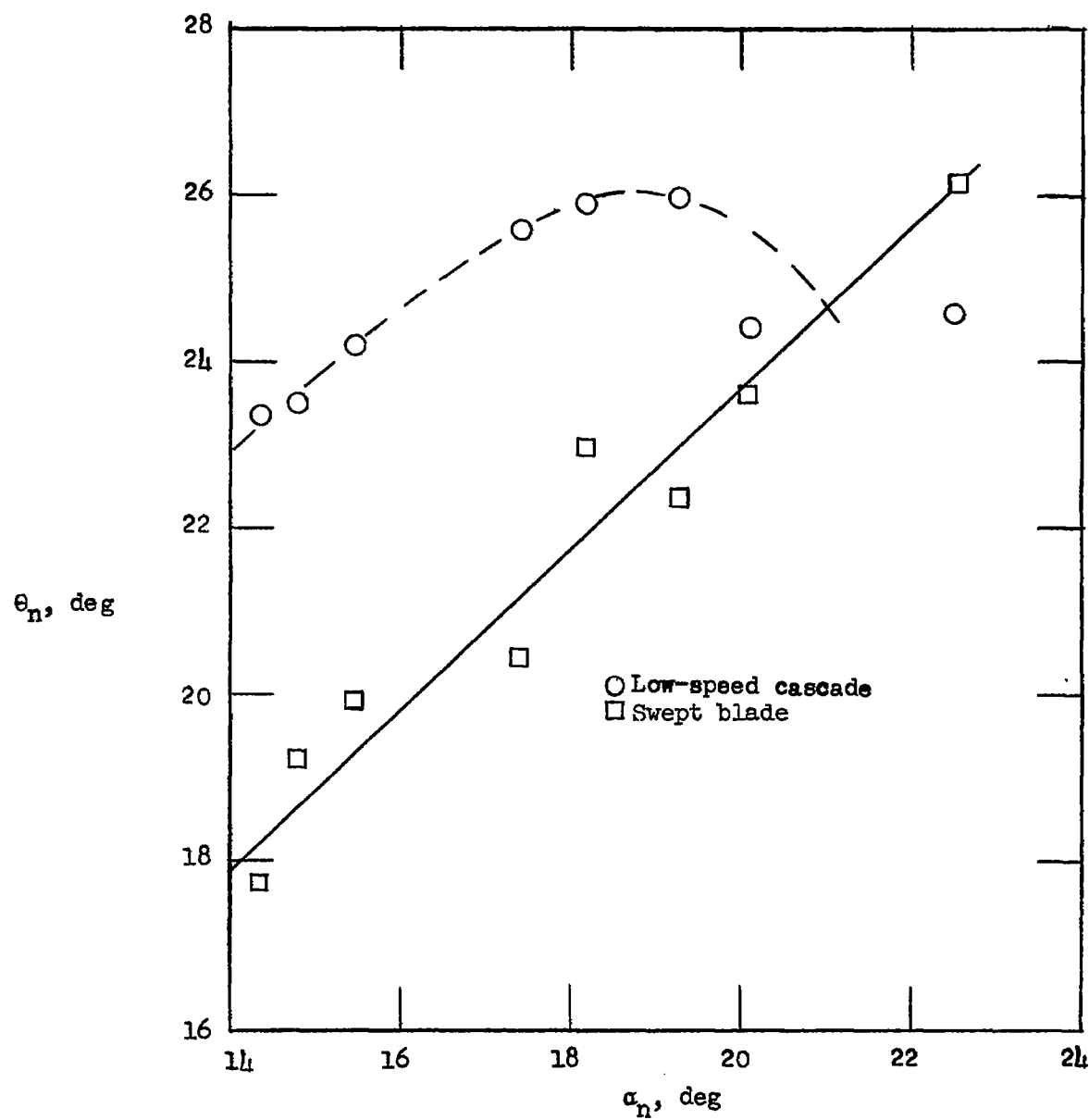
(a) Outboard section.

Figure 13.- Turning angle against angle of attack, using sections normal to the leading edge.



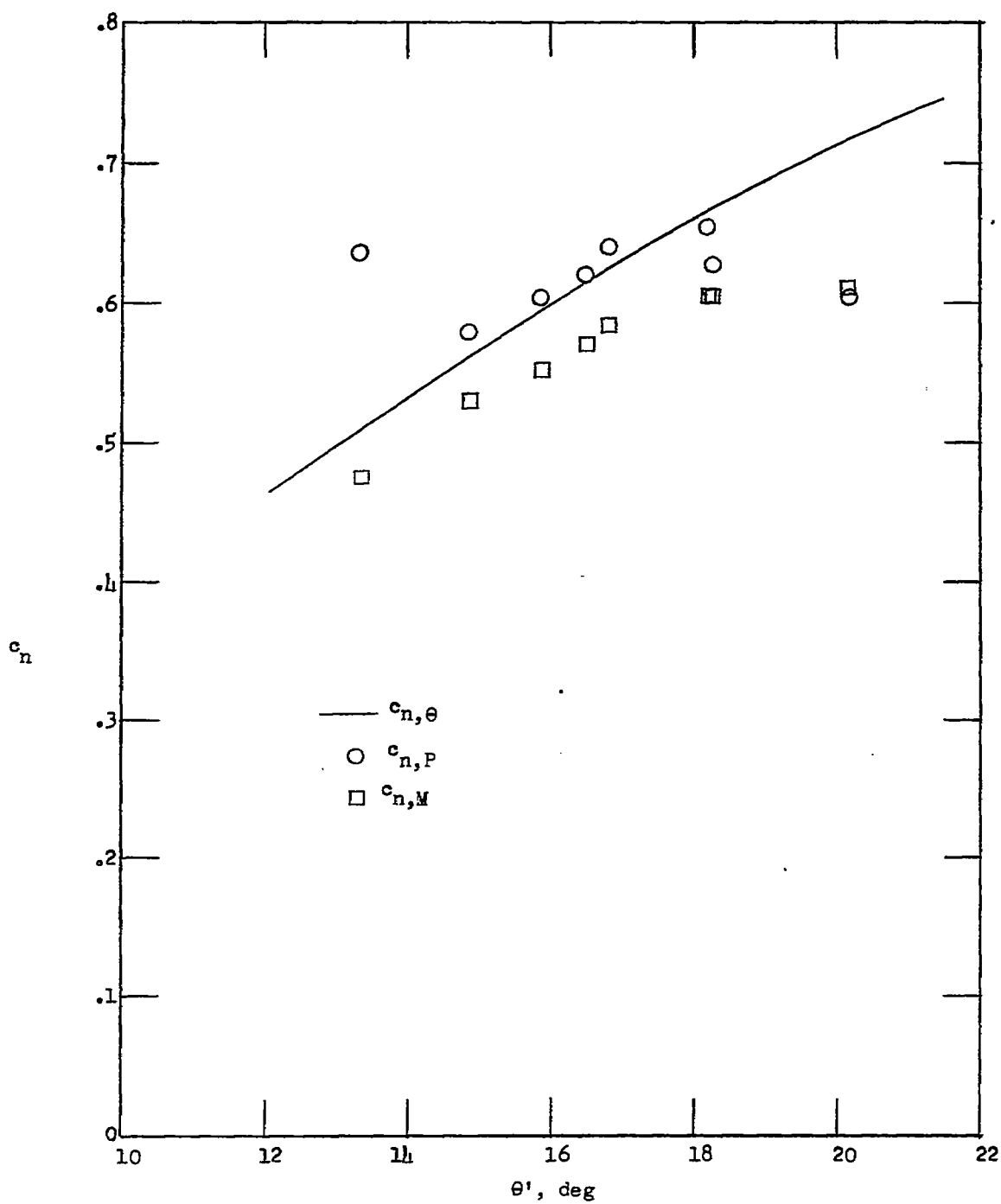
(b) Mean section.

Figure 13.- Continued.



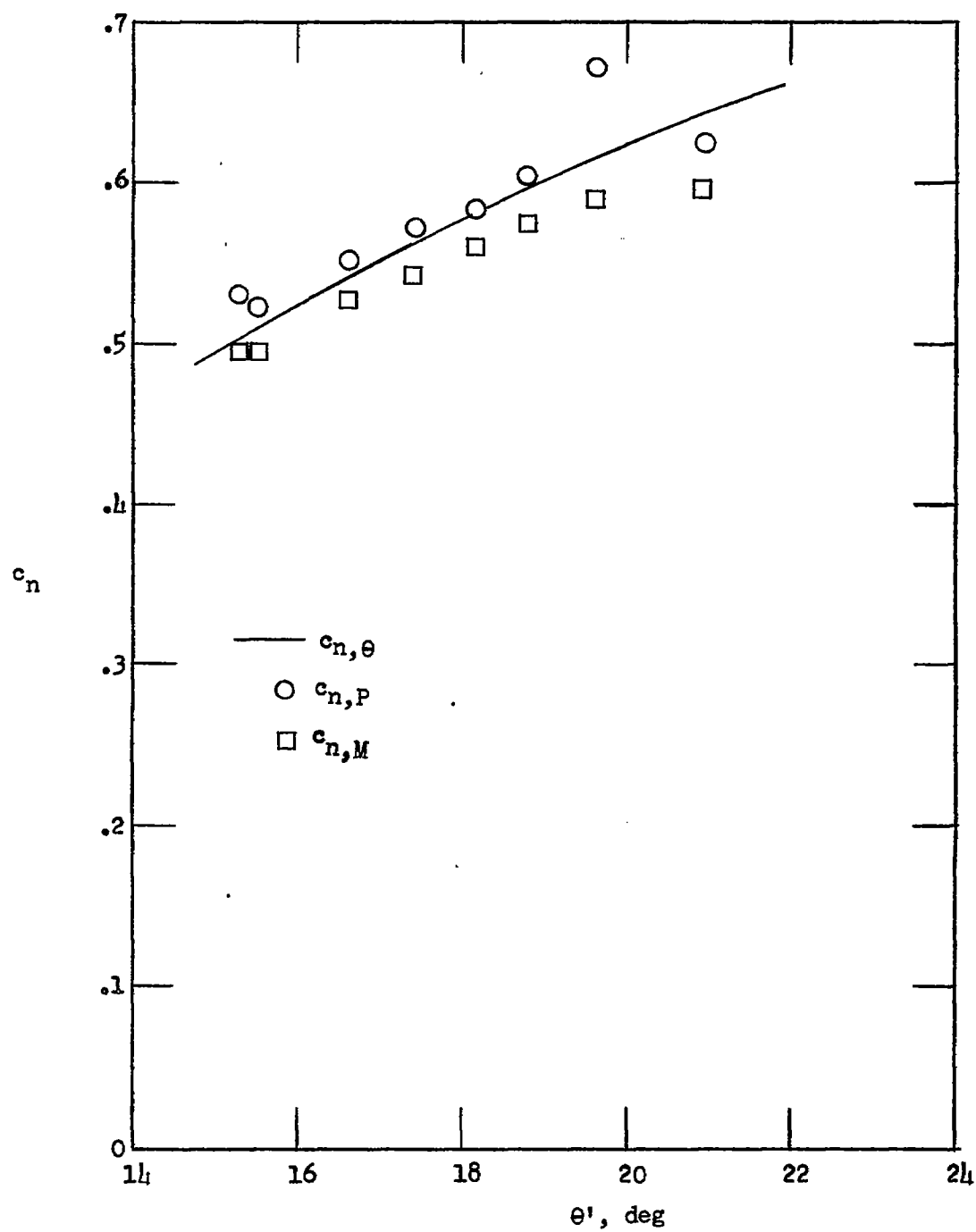
(c) Inboard section.

Figure 13.- Concluded.



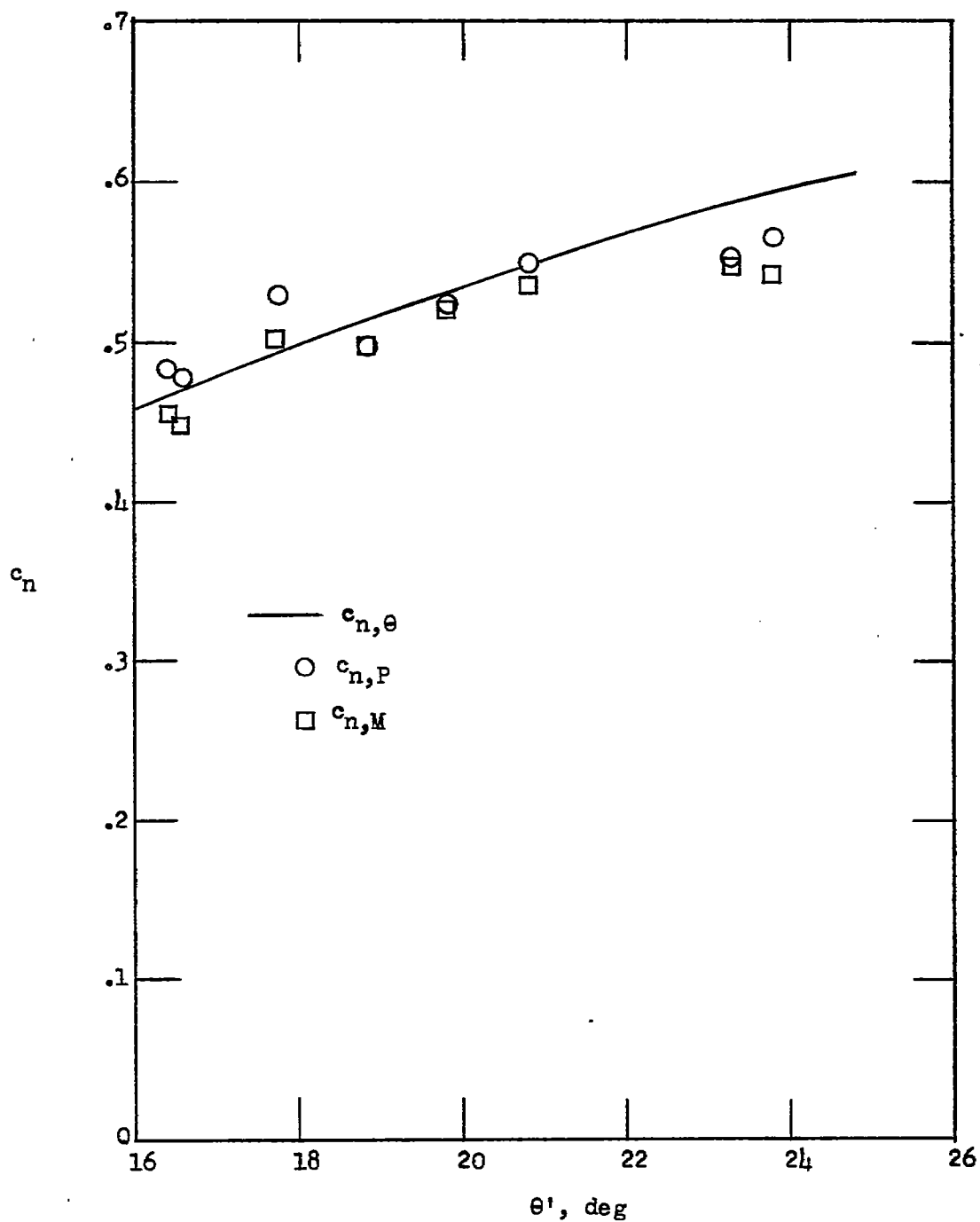
(a) Outboard section.

Figure 14.- Section normal-force coefficient against turning angle.



(b) Mean section.

Figure 14.- Continued.



(c) Inboard section.

Figure 14.- Concluded.